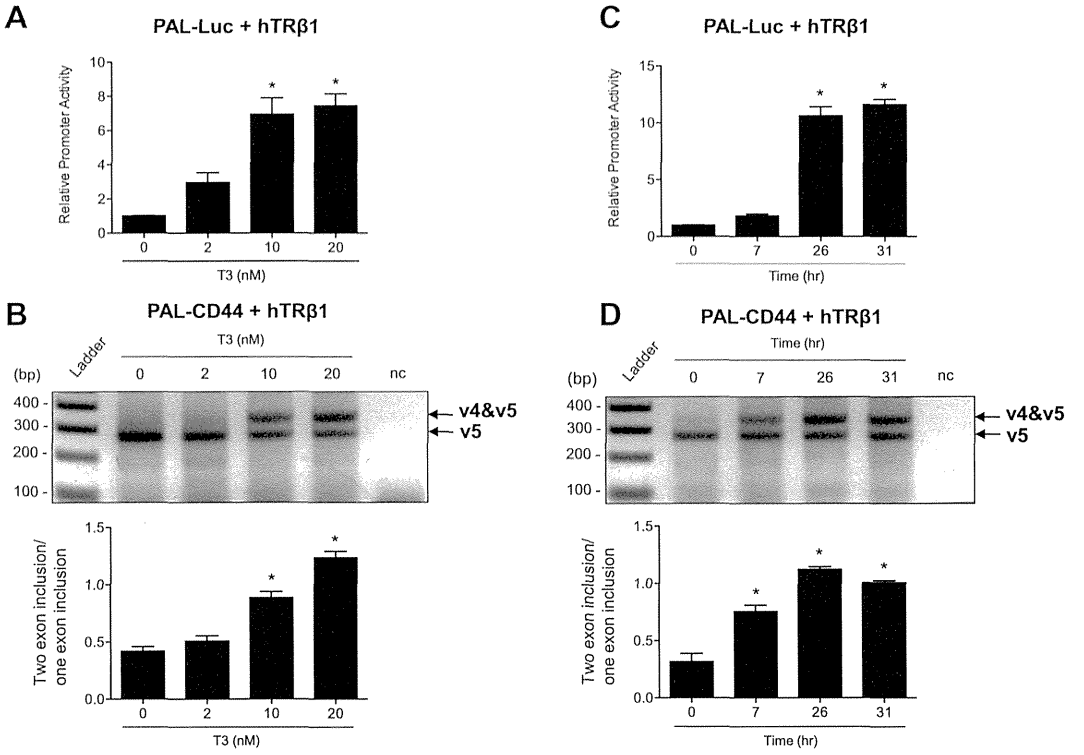

Fig. 2. T3 in the presence of cotransfected TR stimulated the two-exon inclusion of the PAL-CD44 in parallel with the increased transcription of PAL-Luc in a dose- and time-dependent manner. pGL4.23 PAL-Luc or pGL4.23 PAL-CD44 was cotransfected with TRβ1 expression vector, and luciferase assays (Fig. 2A and C) and AS minigene assays (Fig. 2B and D) were performed after treatment with indicated concentrations of T3 during indicated time periods. Luciferase assay data represent the mean ± SEM from triplicate samples. Representative agarose gels are shown (Fig. 2B and D, upper panels). Molecular size markers (Ladder) are indicated as base pairs (bp). Arrows indicate PCR products containing v4 and V5 or v5. Band intensities were quantitated and the ratio of two-exon included RNA to one-exon included RNA was expressed as the mean ± SEM from triplicate PCR samples. Asterisks indicate significant differences from 0. nc represents PCR samples without the cDNA template. Experiments were repeated with similar results.

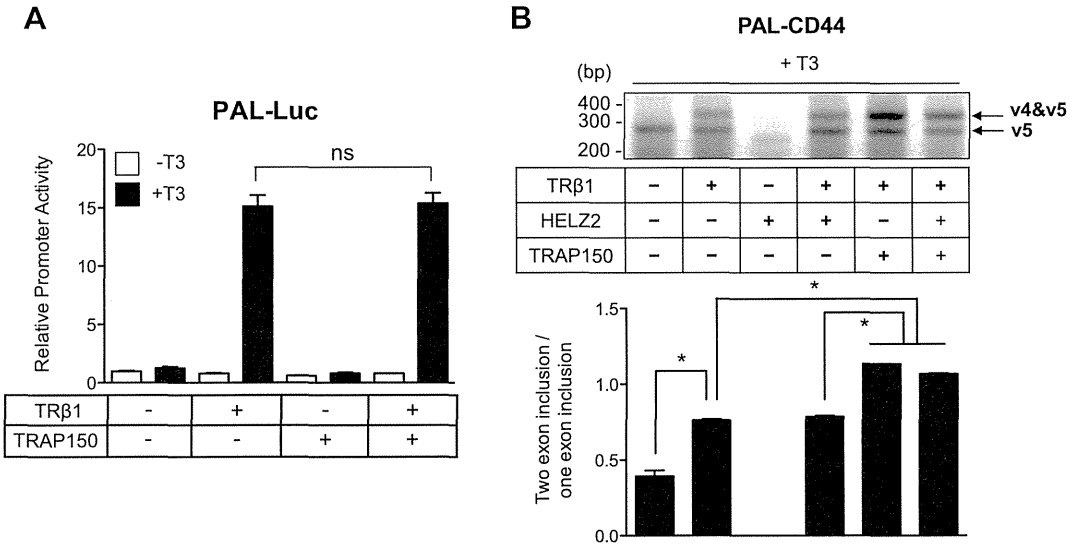

Fig. 3. TRAP150 did not stimulate the transcription of PAL-Luc, but increased the two-exon inclusion of the PAL-CD44 minigene. PAL-Luc or PAL-CD44 was cotransfected in the presence or absence of TRβ1 with or without the TRAP150 expression vector. Luciferase and minigene assays were performed 24 h after the incubation with 10 nM T3(Figs. 3A and 3B). Data are expressed as in Fig. 2. Experiments were repeated twice with similar results. Asterisks indicate significant differences between the indicated groups. ns; not significant.

processing factors to the CTD [1,2]. In addition, certain pre-mRNA processing factors, including PSF, have been shown to associate with pol IIa-containing holoenzyme complexes [34]. Sequence-specific DNA-binding transcription factors and their associating TCRs play important roles in the recruitment of the pol II holoenzyme complex to promoter regions [9], and the types of promoters

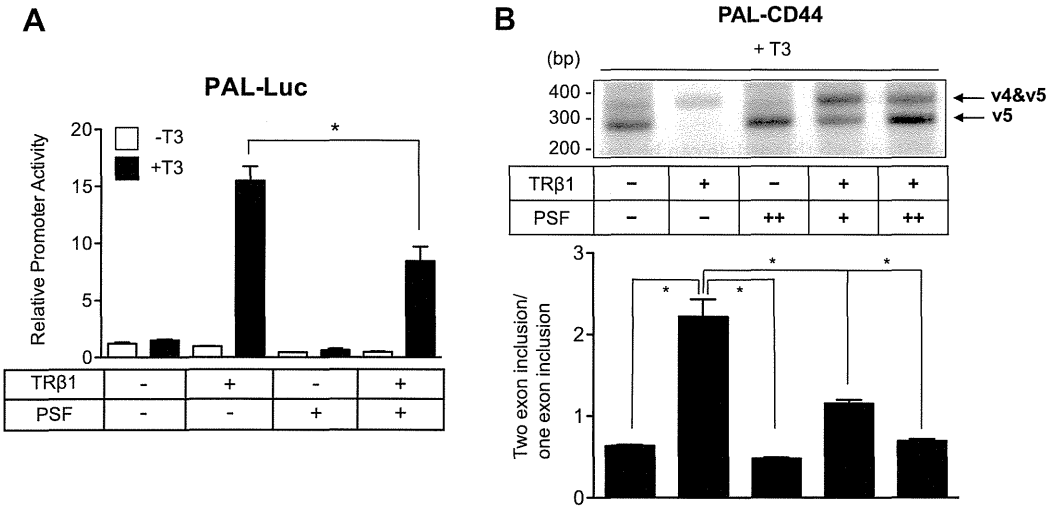

Fig. 4. PSF repressed the transcription of PAL-Luc and two-exon inclusion of the PAL-CD44 minigene. PAL-Luc or PAL-CD44 was cotransfected in the presence or absence of TRβ1 with or without the PSF expression vector. Data from luciferase assays (A) and minigene assays (B) are shown as in Fig. 3. Experiments were repeated twice with similar results.

or promoter-bound activators used to drive transcription can influence the efficiency of pre-mRNA processing steps in corresponding transcribed RNAs [1,2].

In the present study, we showed that liganded TR could stimulate gene transcription in parallel with the two-exon inclusion of the CD44 minigene driven by the minimal promoter under the control of PAL-TRE. However, the present results differed from those reported previously in which a reduction was observed in two-exon inclusion using a CD44 minigene driven by a mouse mammary tumor virus promoter in the presence of liganded PR or a minimal promoter carrying the estrogen responsive element in the presence of liganded ER [13]. Therefore, the types of promoters and recruited NR could affect AS decisions by changing the RNA elongation rate and/or recruitment of different splicing factors, as described previously [1,2]. The AS decision of the CD44 minigene driven by the CMV promoter, which lacks positive TRE, was not affected by the cotransfected TR in the present study, suggesting that TRE-bound TR could co-transcriptionally modulate AS of the CD44 minigene driven by PAL-TRE.

T3-induced two-exon inclusion was significantly increased by the cotransfection of TRAP150 in the present study. TRAP150 was initially identified as a subunit of the TRAP/Mediator multi-protein complex, which has been reported to bridge DNA-bound liganded NRs and the basal transcription machinery [20]. TRAP150 possesses an arginine/serine rich domain, which is an RNA recognition motif that is characteristic of the serine–arginine protein family involved in pre-mRNA splicing [21]. TRAP150 has been shown to associate with spliceosomes in transient and heparin-sensitive manners [35], may be recruited to emerging transcripts via an interaction with pol II-associated splicing factors such as CA150 during transcription [36,37], and activates pre-mRNA splicing *in vivo* [21]. Med23, another subunit of the TRAP/Mediator complex, has recently been shown to regulate AS through an interaction with heterogeneous ribonucleoprotein L and the splicing machinery [38]. The present results provide supportive evidence that specific components of the TRAP/Mediator complex, in addition to other classes of NR coregulators including PPARγ coactivator 1, p72, CoAA, CAPER, and Sam68 [12–16], could play a novel role in coupling transcription with AS in NR-mediated gene regulation.

PSF has previously been shown to function as a transcriptional corepressor of several NRs including TR by recruiting histone deacetylases via direct interactions with Sin3A [26,28]. In contrast to the NR corepressor that dissociates from TR in the presence of T3 [17], PSF could associate with the DNA-binding domain of TR in the absence and presence of T3 [26]. In the present study, the overexpression of PSF significantly reduced the two-exon inclusion of the TRE-driven CD44 minigene in the presence of cotransfected TR. PSF possesses two canonical RNA-recognition motifs [24] and has been suggested to play important roles in RNA processing [39,40]. PSF has subsequently been shown to associate with transcription initiation and elongation complexes and is also capable of directly interacting with the CTD of both pol IIa and IIo [34]. PSF can be co-purified with the activation domain of VP16 and stimulate VP16-dependent pre-mRNA processing via an interaction with the pol II CTD [41]. Heyd et al. recently demonstrated that PSF phosphorylated by glycogen synthase kinase 3 (GSK3) could stably associate with TRAP150 in resting T cells. By reducing GSK3 activity upon T cell activation, the dephosphorylated form of PSF could dissociate from TRAP150 and bind to the exonic splicing silencer element, thereby repressing exon inclusion of the CD45 gene [22]. Taken together, these findings suggest that PSF could play an important role in coupling alternative pre-mRNA splicing with gene transcription. Because the overexpression of PSF significantly attenuated the T3-induced transcription of PAL-Luc by TR, but did not reduce the two-exon inclusion of the CMV-CD44 minigene in the present study, we speculated that the reduction in the two-exon inclusion of the PAL-CD44 minigene by PSF may be mainly caused by its corepressor activity for TR-mediated gene transcription. The present study collectively demonstrated that TR could co-transcriptionally modulate alternative pre-mRNA splicing, similar to other NRs, in collaboration with its associating coregulators [12–16].

Conflict of interest

The authors have nothing to disclose.

Acknowledgments

We thank Drs. B.W. O'Malley (Baylor College of Medicine) and S. Kawamoto (National Institute of Health) for providing the CMV-CD44 minigene and PSF expression vector, respectively. This work

was supported by Development for New Research Awards from the Japan Thyroid Association to TS.

Appendix A. Supplementary data

Supplementary data associated with this article can be found, in the online version, at http://dx.doi.org/10.1016/j.bbrc.2014.07.029.

References

[1] K.M. Neugebauer, On the importance of being co-transcriptional, J. Cell Sci. 115 (2002) 3865–3871.
[2] S. Shukla, S. Oberdoerffer, Co-transcriptional regulation of alternative pre-mRNA splicing, Biochem. Biophys. Acta 2012 (1819) 673–683.
[3] E.T. Wang, R. Sandberg, S. Luo, et al., Alternative isoform regulation in human tissue transcriptomes, Nature 456 (2008) 470–476.
[4] J. Tazi, N. Bakkour, S. Stamm, Alternative splicing and disease, Biochim. Biophys. Acta 1792 (2009) 14–26.
[5] A. Piekiełko-Witkowska, A. Nauman, Alternative splicing and its role in pathologies of the endocrine system, Endokrynol. Pol. 62 (2011) 160–170.
[6] J. Boultwood, H. Dolatshad, S.S. Varanasi, et al., The role of splicing factor mutations in the pathogenesis of the myelodysplastic syndromes, Adv. Biol. Regul. 54 (2014) 153–161.
[7] C.K. Glass, Differential recognition of target genes by nuclear receptor monomers dimers, and heterodimers, Endocr. Rev. 15 (1994) 391–407.
[8] R.C. Ribeiro, P.J. Kushner, J.D. Baxter, The nuclear hormone receptor gene superfamily, Annu. Rev. Med. 46 (1995) 443–453.
[9] C.K. Glass, M.G. Rosenfeld, The coregulator exchange in transcriptional functions of nuclear receptors, Genes Dev. 14 (2000) 121–141.
[10] D.M. Lonard, R.B. Lanz, B.W. O'Malley, Nuclear receptor coregulators and human disease, Endocr. Rev. 28 (2007) 575–587.
[11] D.M. Lonard, B.W. O'Malley, Nuclear receptor coregulators: modulators of pathology and therapeutic targets, Nat. Rev. Endocrinol. 8 (2012) 598–604.
[12] M. Monsalve, Z. Wu, G. Adelmant, et al., Direct coupling of transcription and mRNA processing through the thermogenic coactivator PGC-1, Mol. Cell 6 (2000) 307–316.
[13] D. Auboeuf, A. Hönig, S.M. Berget, et al., Coordinate regulation of transcription and splicing by steroid receptor coregulators, Science 298 (2002) 416–419.
[14] D.H. Dowhan, E.P. Hong, D. Auboeuf, et al., Steroid hormone receptor coactivation and alternative RNA splicing by $U2AF^{65}$-related proteins CAPERα and CAPERβ, Mol. Cell 17 (2005) 429–439.
[15] J. Sun, A.L. Blair, S.E. Aiyar, et al., Cofactor of BRCA1 modulates androgen-dependent transcription and alternative splicing, J. Steroid Biochem. Mol. Biol. 107 (2007) 131–139.
[16] P. Rajan, L. Gaughan, C. Dalgliesh, et al., The RNA-binding and adaptor protein Sam68 modulates signal-dependent splicing and transcriptional activity of the androgen receptor, J. Pathol. 215 (2008) 67–77.
[17] M.A. Lazar, Thyroid hormone action: a binding contract, J. Clin. Invest. 112 (2003) 497–499.
[18] M.J. Latasa, B. Belandia, A. Pascual, Thyroid hormones regulate beta-amyloid gene splicing and protein secretion in neuroblastoma cells, Endocrinology 139 (1998) 2692–2698.
[19] D.C. Timmer, O. Bakker, W.M. Wiersinga, Triiodothyronine affects the alternative splicing of thyroid hormone receptor alpha mRNA, J. Endocrinol. 179 (2003) 217–225.
[20] J.D. Fondell, H. Ge, R.G. Roeder, Ligand induction of a transcriptionally active thyroid hormone receptor coactivator complex, Proc. Natl. Acad. Sci. U.S.A. 93 (1996) 8329–8333.
[21] K.M. Lee, W. Hsu Ia, W.Y. Tarn, TRAP150 activates pre-mRNA splicing and promotes nuclear mRNA degradation, Nucleic Acids Res. 38 (2010) 3340–3350.
[22] F. Heyd, K.W. Lynch, Phosphorylation-dependent regulation of PSF by GSK3 controls CD45 alternative splicing, Mol. Cell 40 (2010) 126–137.
[23] K. Horiuchi, T. Kawamura, H. Iwanari, et al., Identification of Wilms' tumor 1-associating protein complex and its role in alternative splicing and the cell cycle, J. Biol. Chem. 288 (2013) 33292–33302.
[24] J.G. Patton, E.B. Porro, J. Galceran, et al., Cloning and characterization of PSF, a novel pre-mRNA splicing factor, Genes Dev. 7 (1993) 393–406.
[25] P. Close, P. East, A.B. Dirac-Svejstrup, et al., DBIRD complex integrates alternative mRNA splicing with RNA polymerase II transcript elongation, Nature 484 (2012) 386–389.
[26] M. Mathur, P.W. Tucker, H.H. Samuels, PSF is a novel corepressor that mediates its effect through Sin3A and the DNA binding domain of nuclear hormone receptors, Mol. Cell. Biol. 21 (2001) 2298–2311.
[27] X. Dong, O. Shylnova, J.R. Challis, et al., Identification and characterization of the protein-associated splicing factor as a negative co-regulator of the progesterone receptor, J. Biol. Chem. 280 (2005) 13329–13340.
[28] X. Dong, J. Sweet, J.R. Challis, et al., Transcriptional activity of androgen receptor is modulated by two RNA splicing factors, PSF and p54nrb, Mol. Cell. Biol. 27 (2007) 4863–4875.
[29] A. Katano-Toki, T. Satoh, T. Tomaru, et al., THRAP3 interacts with HELZ2 and plays a novel role in adipocyte differentiation, Mol. Endocrinol. 27 (2013) 769–780.
[30] T. Tomaru, T. Satoh, S. Yoshino, et al., Isolation and characterization of a transcriptional cofactor and its novel isoform that bind the deoxyribonucleic acid-binding domain of peroxisome proliferator-activated receptor-gamma, Endocrinology 147 (2006) 377–388.
[31] K.K. Kim, Y.C. Kim, R.S. Adelstein, S. Kawamoto, Fox-3 and PSF interact to activate neural cell-specific alternative splicing, Nucleic Acids Res. 39 (2011) 3064–3078.
[32] T. Satoh, T. Ishizuka, S. Yoshino, et al., Roles of proteasomal 19S regulatory particles in promoter loading of thyroid hormone receptor, Biochem. Biophys. Res. Commun. 386 (2009) 697–702.
[33] E. Stickeler, S.D. Frase, A. Honig, et al., The RNA binding protein YB-1 binds A/C-rich exon enhancers and stimulates splicing of the CD44 alternative exon v4, EMBO J. 20 (2001) 3821–3830.
[34] A. Emili, M. Shale, S. McCracken, et al., Splicing and transcription-associated proteins PSF and p54nrb/nonO bind to the RNA polymerase II CTD, RNA 8 (2002) 1102–1111.
[35] C. Merz, H. Urlaub, C.L. Will, et al., Protein composition of human mRNPs spliced in vitro and differential requirements for mRNP protein recruitment, RNA 13 (2007) 116–128.
[36] K.T. Lin, R.M. Lu, W.Y. Tarn, The WW domain-containing proteins interact with the early spliceosome and participate in pre-mRNA splicing in vivo, Mol. Cell. Biol. 24 (2004) 9176–9185.
[37] A.C. Goldstrohm, T.R. Albrecht, C. Suñé, et al., The transcription elongation factor CA150 interacts with RNA polymerase II and the pre-mRNA splicing factor SF1, Mol. Cell. Biol. 21 (2001) 7617–7628.
[38] Y. Huang, W. Li, X. Yao, et al., Mediator complex regulates alternative mRNA processing via the MED23 subunit, Mol. Cell 45 (2012) 459–469.
[39] O. Gozani, J.G. Patton, R. Reed, A novel set of spliceosome-associated proteins and the essential splicing factor PSF bind stably to pre-mRNA prior to catalytic step II of the splicing reaction, EMBO J. 13 (1994) 3356–3367.
[40] C.S. Lutz, C. Cooke, J.P. O'Connor, et al., The snRNP-free U1A (SF-A) complex(es): identification of the largest subunit as PSF, the polypyrimidine-tract binding protein-associated splicing factor, RNA 4 (1998) 1493–1499.
[41] E. Rosonina, J.Y. Ip, J.A. Calarco, et al., Role for PSF in mediating transcriptional activator-dependent stimulation of pre-mRNA processing in vivo, Mol. Cell. Biol. 25 (2005) 6734–6746.

Protection Against High-Fat Diet-Induced Obesity in *Helz2*-Deficient Male Mice Due to Enhanced Expression of Hepatic Leptin Receptor

Satoshi Yoshino,* Tetsurou Satoh,* Masanobu Yamada, Koshi Hashimoto, Takuya Tomaru, Akiko Katano-Toki, Satoru Kakizaki, Shuichi Okada, Hiroyuki Shimizu, Atsushi Ozawa, Takafumi Tuchiya, Hayato Ikota, Yoichi Nakazato, Munemasa Mori, Takashi Matozaki, Tsutomu Sasaki, Tadahiro Kitamura, and Masatomo Mori

Departments of Medicine and Molecular Science (S.Y., T.Sat., M.Y., K.H., T.To., A.K.-T., S.K., S.O., H.S., A.O., T.Tu., Ma.Mori) and Human Pathology (H.I., Y.N.), Gunma University Graduate School of Medicine, Maebashi, 371-8511 Japan; Laboratory of Biosignal Sciences (Mu.Mori, T.Ma.) and Metabolic Signal Research Center, Institute for Molecular and Cellular Regulation (T.Sas., T.K.), Gunma University, Maebashi, 371-8512 Japan; and Kitakanto Molecular Novel Research Institute for Obesity and Metabolism (Ma.Mori), Midori, 379-2311 Japan

Obesity arises from impaired energy balance, which is centrally coordinated by leptin through activation of the long form of leptin receptor (Leprb). Obesity causes central leptin resistance. However, whether enhanced peripheral leptin sensitivity could overcome central leptin resistance remains obscure. A peripheral metabolic organ targeted by leptin is the liver, with low *Leprb* expression. We here show that mice fed a high-fat diet (HFD) and obese patients with hepatosteatosis exhibit increased expression of hepatic helicase with zinc finger 2, a transcriptional coactivator (*Helz2*), which functions as a transcriptional coregulator of several nuclear receptors, including peroxisome proliferator-activated receptor γ in vitro. To explore the physiological importance of Helz2, we generated *Helz2*-deficient mice and analyzed their metabolic phenotypes. *Helz2*-deficient mice showing hyperleptinemia associated with central leptin resistance were protected against HFD-induced obesity and had significantly up-regulated hepatic Leprb expression. *Helz2* deficiency and adenovirus-mediated liver-specific exogenous Leprb overexpression in wild-type mice significantly stimulated hepatic AMP-activated protein kinase on HFD, whereas *Helz2*-deficient *db/db* mice lacking functional Leprb did not. Fatty acid-β oxidation was increased in *Helz2*-deficeint hepatocytes, and *Helz2*-deficient mice revealed increased oxygen consumption and decreased respiratory quotient in calorimetry analyses. The enhanced hepatic AMP-activated protein kinase energy-sensing pathway in *Helz2*-deficient mice ameliorated hyperlipidemia, hepatosteatosis, and insulin resistance by reducing lipogenic gene expression and stimulating lipid-burning gene expression in the liver. These findings together demonstrate that *Helz2* deficiency ameliorates HFD-induced metabolic abnormalities by stimulating endogenous hepatic Leprb expression, despite central leptin resistance. Hepatic HELZ2 might be a novel target molecule for the treatment of obesity with hepatosteatosis. **(*Endocrinology* 155: 3459–3472, 2014)**

ISSN Print 0013-7227 ISSN Online 1945-7170
Printed in U.S.A.

Received December 20, 2013. Accepted June 28, 2014.
First Published Online July 8, 2014

* S.Y. and T.Sat. contributed equally to this work.

Abbreviations: Ab, antibody; ACC, acetyl-coenzyme A carboxylase; AMPK, AMP-activated protein kinase; BAT, brown adipose tissue; bw, body weight; CBP, cyclic AMP response element binding protein-binding protein; EGFP, enhanced green fluorescent protein; FA, fatty acid; HA, human influenza hemagglutinin; HELZ2, helicase with zinc finger 2, a transcriptional coactivator; HFD, high-fat diet; KO, knockout; Leprb, leptin receptor; ND, normal diet; NEO, neomycin cassette; NR, nuclear receptor; p, phosphorylated; PGC-1α, PPARγ coactivator-1α; PPAR, peroxisome proliferator-activated receptor; qRT-PCR, quantitative RT-PCR; RQ, respiratory quotient; sh*Helz2*, *Helz2*-specific shRNA; shRNA, short hairpin RNA; SRC, steroid receptor coactivator; STAT3, signal transducer and activator of transcription-3; TG, triglyceride; VO_2, oxygen consumption; WAT, white adipose tissue; WT, wild type.

Obesity has long been of concern as a health risk factor and is the epidemic cause of dyslipidemia, hepatosteatosis, type 2 diabetes mellitus, cardiovascular disease, and some types of cancers on a worldwide level (1, 2). Obesity develops from impaired energy homeostasis pathways. These pathways include the regulation of food intake by the central hypothalamus and energy expenditure in peripheral metabolic tissues, which includes energy expenditure during physical activity, energy expenditure by metaboloregulatory thermogenesis, and mandatory energy expenditure through basic cellular functions (3–5).

Leptin is an adipose-derived hormone (6) involved in regulating energy homeostasis via the activation of the long form of leptin receptor (Leprb) (7), which is expressed in the central hypothalamus and peripheral metabolic tissues at high and low levels, respectively. The liver functions as the main regulator of energy homeostasis after peripheral stimulation by leptin (8, 9). Obese patients are considered leptin resistant, which involves central and peripheral tissues resistant to endogenous and exogenously administered leptin (10, 11). These patients showed decreased expression of hepatic *Leprb* (12), whose knockout, however, caused no metabolic changes in mice fed regular chow (13). Increased expression of hypothalamic Leprb was speculated to cause hypersensitivity to central leptin action (14). In line with this view, liver-specific overexpression of exogenous Leprb in *Leprb*-deficient *fa/fa* rats improves peripheral metabolic abnormalities without altering food intake (15), suggesting that the increased expression of endogenous Leprb in the liver could ameliorate peripheral leptin resistance, regardless of central leptin resistance. However, little is known about endogenous factors that regulate hepatic Leprb expression, and whether enhanced peripheral leptin sensitivity in obesity could overcome central leptin resistance remains obscure.

Peroxisome proliferator-activated receptor (PPAR)γ belongs to the nuclear receptor (NR) superfamily and is a ligand-dependent transcriptional factor involved in adipocyte differentiation as well as glucose and lipid metabolism in the body (16–18). NRs require a variety of coregulators with diverse enzymatic activities to exert their full transcriptional effects (19, 20). In addition to NRs themselves, emerging evidence indicates that several coregulators for NRs participate closely in the regulation of energy homeostasis. For instance, steroid receptor coactivator-1 (SRC-1), steroid receptor coactivator-2 (SRC-2), cyclic AMP response element binding protein-binding protein (CBP), and PPARγ coactivator-1α (PGC-1α) are involved in hepatic metabolic functions (19, 20). Using the DNA-binding domain and part of the hinge region of PPARγ as bait in a yeast 2-hybrid screen, we isolated helicase with zinc finger 2, a transcriptional coactivator (HELZ2) (previously designated as PPARγ DNA-binding domain-interacting protein1 or PPARα-interacting complex 285 kDa protein 285, accession number AF517673.1), which functions as a coregulator of PPARs and other NRs in vitro (21, 22). Mouse Helz2, consisting of 2948 amino acids, possesses characteristic structures, including 2 ATP-binding motifs, a region homologous to the catalytic domain of ribonuclease B, and dual DNA/RNA helicase motifs similar to human HELZ2, and structurally belongs to the DNA2/ATP-dependent RNA helicase NAM7 helicase family involved in gene transcription, RNA processing, and DNA repair (23, 24). We recently showed that Helz2 could be involved in terminal differentiation of 3T3-L1 cells in cooperation with thyroid hormone receptor-associated protein 3, a component of the Mediator complex (25). However, the physiological significance of Helz2 remains to be explored. To gain insight into the physiological roles of Helz2, we generated *Helz2*$^{-/-}$ (knockout, KO) mice and examined whether Helz2 could be involved in energy homeostasis under high-fat diet (HFD) conditions in the present study. We found that *Helz2* deficiency improves HFD-induced metabolic abnormalities in association with enhanced expression of Leprb in the liver.

Materials and Methods

Animals

The Institutional Animal Care and Use Committee of Gunma University approved all animal protocols. To generate *Helz2* KO mice, a targeting vector substituting the neomycin cassette (NEO) for exons 1–6 of the mouse *Helz2* gene was constructed. Chimera mice were generated by the standard homologous recombination technique and were backcrossed with C57BL/6 mice to obtain F1 heterozygous KO mice. Heterozygous mice were then mated to obtain *Helz2* KO mice. The backcross was repeated, and F6–F8 KO mice and their wild-type (WT) littermates were used for subsequent analyses. Two independent KO mouse lines were established, and their phenotypes were identical in subsequent analyses. Mice were housed in a temperature-controlled room with a 12-hour light, 12-hour dark cycle and fed ad libitum on normal diet (ND) with 4.7% (wt/wt) fat (CLEA Rodent Diet CE-2; Clea Japan, Inc). For HFD feeding, a diet containing 60% (wt/wt) fat (Oriental Yeast Co, Ltd) was given after weaning as described previously (26). Daily food intake was measured. Male and female *db*/+ mice with a C57BL/6 background were purchased from Charles River Laboratory Service and mated with *Helz2* KO mice to generate *Helz2-null db/db* mice.

Human liver specimens

The Ethics Committee of Gunma University Hospital on Human Research approved the clinical study. Written informed consent was obtained from all subjects. Liver specimens from obese patients were obtained by echo-guided needle biopsies,

and total RNA was isolated and subjected to quantitative RT-PCR (qRT-PCR). Liver samples consist of controls (35.6 ± 3.0 y old, male vs female = 7:3) and hepatosteatosis (nonalcoholic steatohepatitis, 35.3 ± 2.5 y old, male vs female = 6:4), all of which were confirmed histologically in hepatic biopsy specimens.

Genotyping and Southern and Northern blot analyses

Genomic DNA was isolated from the tail of each mouse and subjected to PCR for genotyping. The nucleotide sequences of the primers used were *Helz2* forward, 5′-ATGCAGGTCACAC-CTAGGCTCTTC-3′, NEO forward, 5′-TGCGAGGCCA-GAGGCCACTTGTGTAGC-3′, and common reverse, 5′-TTCAGGCCATG CTCTAGGTCAAG-3′. PCR was performed for 35 cycles. Genomic DNA was digested with *Bam*HI and subjected to Southern blot analysis using a [^{32}P]-labeled partial fragment of mouse *Helz2* cDNA as we described previously (21). Mice were killed by cervical dislocation, and tissues were excised, weighed, and snap frozen in liquid nitrogen. Total RNA was isolated from livers and other tissues, and Northern blot analysis was performed using a [^{32}P]-labeled mouse *Helz2* cRNA probe as described previously (21). The genotype of *db/db* mice was verified by direct sequencing of genomic PCR products of the *Lepr* gene. Forward and reverse PCR primers for the *Lepr* gene were 5′-AGAACGGACACTCTTTGAAGTCTC-3′ and 5′-CG-GATTTCATTACGGTGGT-3′, respectively.

cDNA microarray analysis

cDNA microarray analysis using Affymetrix's mouse GeneChip was performed on hepatic RNAs from WT and KO mice fed HFD.

Quantitative RT-PCR

qRT-PCR was performed as described previously (27) using primers for the genes encoding murine Lepra, Leprb, Ppars, and coregulators and genes associated with lipid synthesis and fatty acid (FA) oxidation. Amplification was normalized by parallel qRT-PCR of glyceraldehyde-3-phosphate dehydrogenase mRNA. The nucleotide sequences of the primers used are summarized in Supplemental Table 1.

Immunoblot analyses

Whole-cell lysates were prepared, and protein concentrations were measured as described (21, 25). Samples were separated by SDS-PAGE and transferred to polyvinylidene difluoride membranes (GE Healthcare UK, Ltd). Immunoblotting was performed overnight at 4°C. Anti-Lepr antibody (Ab) (sc1834-R) was purchased from Santa Cruz Biotechnology, Inc; those for AMP-activated protein kinase (AMPK)α (number 2532), phosphorylated (p)Thr172-AMPKα (number 2531), acetyl-coenzyme A carboxylase (ACC) (number 3676), pSer79-ACC (number 3661), signal transducer and activator of transcription-3 (STAT3) (number 9132), pTyr705-STAT3 (number 9131), Akt (number 9272), and pSer472-Akt (number 9271) were from Cell Signaling Technology, Inc; an anticyclophilin A Ab was from Upstate Biotechnology, Inc; and an antiglyceraldehyde-3-phosphate dehydrogenase Ab (clone6c5, ab8245) was from Abcam. Membranes were incubated with a horseradish peroxidase-conjugated secondary Ab (GE Healthcare), and signals were detected using ECL plus reagent (GE Healthcare) and analyzed using an image analyzer (Molecular Imager FX; Bio-Rad Laboratories, Inc).

Biochemical parameters and insulin and glucose tolerance tests

Mice were fasted for 16 hours before blood samples were drawn. Enzymatic kits were used to measure serum insulin and leptin (Ultrasensitive insulin or leptin ELISA kit; Morinaga Institute of Biological Science, Inc) and adiponectin (mouse/rat adiponectin ELISA kit; Otsuka Pharmaceutical Co, Ltd). Blood glucose levels were determined using an enzymatic method. Serum lipid profiles were quantitated by gel filtration HPLC analysis (Skylight Biotech). Triglyceride (TG) contents in livers were measured by the method previously described (28). Mice received ip injection of insulin (0.5 U of Novo-regular insulin/kg body weight [bw]) or glucose (1.0 g glucose/kg bw), and subsequent blood samples were used to determine blood glucose levels.

Construction of adenoviruses

Adenovirus encoding EGFP was generated from pAd-enhanced green fluorescent protein (EGFP) as a control. As described previously (29), an adenoviral RNA interference construct was generated from pAd-EGFP containing mouse *Helz2*-specific short hairpin RNA (shRNA) (sh*Helz2*) encoding 5′-GGACAGAGCTGAACCAAAT-3′. The control adenoviral vector was also constructed from pAd-EGFP containing a scrambled sequence of sh*Helz2*: 5′-AACGGATAAACGCGACGTA-3′. Each mouse fed HFD for 20 weeks received tail-vein injection of the adenovirus encoding sh*Helz2* at a dose of 1×10^9 plaque-forming units per mouse. Adenovirus expressing *Leprb* was produced using the AdEasy recombinant adenoviral system as described previously (30). The 3′ fragment of the HA-*Leprb* sequence was excised from pCI-human influenza hemagglutinin (HA)-Leprb with *Kpn*I/*Sal*I and ligated into pAdTrackCMV at *Kpn*I/*Xho*I sites. The 5′ fragment of HA-Leprb was PCR amplified and ligated into pAdTrackCMV-(3′)HA-Leprb vector at *Bg*-*l*II/*Xho*I sites, yielding pAdTrackCMV-HA-Leprb. pAd-HA-Leprb cosmid vector was subsequently generated, and HA-Leprb adenovirus was produced in transfected HEK293 cells and purified from cell extracts by banding on a CsCl gradient. The viral titer was determined by the number of GFP-positive cells generated after infection of serially diluted viruses. The adenoviruses expressing Leprb or EGFP were injected every 6 days for 4 weeks.

Primary hepatocyte culture and transient transfection

Hepatocytes were prepared from WT and KO mice fed HFD using the collagenase-perfusion method with minor modifications and cultured in DMEM containing 10% fetal bovine serum, 0.5 μg/mL insulin, 1μM dexamethasone, 10 ng/mL epidermal growth factor, 200μM ascorbic acid, 10mM nicotine amide, 10 U/mL penicillin, and 10 μg/mL streptomycin (Primary Cell Co, Ltd). Cells were cultured in serum-free DMEM for 3 hours, and whole-cell lysates were prepared at the time points indicated after treatment with regular insulin or mouse leptin (R&D Systems).

Measurement of FA oxidation

The rate of FA oxidation in tissues was examined as described previously (31). [^{14}C]-palmitate was incubated with tissue homogenates at 37°C for 60 minutes, and aquasol in each sample was measured for [^{14}C] counts.

Measurement of oxygen consumption (VO_2) and body temperature

Analysis of gaseous exchange in open-circuit indirect calorimetry was performed using an O_2/CO_2 metabolism measuring system for small animals (MK-5000RQ; Muromachi-Kikai) as described previously (31). The system monitored VO_2 and carbon dioxide production at 3-minute intervals and calculated the respiratory quotient (RQ) ratio (carbon dioxide production/VO_2). To measure resting energy expenditure, mice were placed individually in a chamber equipped with an activity monitoring system (Model Supermex; Muromachi-Kikai). Energy expenditure in each mouse is expressed as per bw with fat mass subtracted. Body temperature was measured using a thermometer (BAT7001H; Physitemp).

Histology

Tissue sections were prepared and immunohistochemistry was performed as described (27) and analyzed microscopically.

Statistical analyses

Data are expressed as the mean ± SEM and were evaluated for statistical significance by ANOVA, Student's *t* test, or the Wilcoxon/Kruskal-Wallis test.

Results

Helz2-deficient mice are protected from HFD-induced obesity

To explore the physiological significance of Helz2, *Helz2* KO mice were generated using a standard homologous recombination technique. Proper recombination was confirmed by genomic Southern blot analyses. The expression of *Helz2* mRNA in the liver of *Helz2*$^{+/-}$ mice was decreased by 50% and was absent in *Helz2*$^{-/-}$ mice in Northern blot analyses. Immunohistochemistry revealed that Helz2 protein was not detected in the nuclei of hepatocytes in *Helz2*$^{-/-}$ mice. Genotyping analyses revealed that *Helz2*$^{+/-}$ mice and *Helz2*$^{-/-}$ mice were born in the expected Mendelian ratio (Figure 1, A–D, and data not shown). Male and female (data not shown) *Helz2* KO mice fed ND developed normally and were fertile throughout adulthood (Figure 1E). Male mice were used for further analyses. No significant changes in food intake, bw gain, or locomoter activities were observed between KO mice and their WT littermates (Figure 1, F–H). In addition, no significant differences were noted in levels of fasting blood glucose, insulin, leptin, or adiponectin (Figure 1I).

Because no apparent metabolic change was observed in *Helz2* KO mice on ND, we next fed KO mice with an HFD containing 60% (wt/wt) fat after weaning and analyzed their metabolic parameters. Body weight progressively increased in WT mice fed HFD but was significantly attenuated in *Helz2* KO mice after 15 weeks of age (Figure 1J). There was less fat deposition in *Helz2* KO mice (Figure 1K), in which body length, food intake (Figure 1, E and F), and locomotor activities (Figure 1L) remained unchanged. *Helz2* deficiency significantly reduced levels of fasting glucose and insulin but sustained hyperleptinemia despite reduced adiposity (Figure 1M). These findings demonstrate that *Helz2* KO mice were protected against HFD-induced obesity, and neither feeding amounts regulated by the hypothalamus nor energy dissipation in the muscle during physical activity could explain the antiobesity effect in *Helz2* deficiency.

Expression of *Helz2* was up-regulated in fatty liver of mice and human

To explore the mechanism underlying the antiobesity effect of *Helz2* deficiency, we first examined expression levels of *Helz2* mRNA in metabolic tissues of WT mice on ND. Northern blot and qRT-PCR analyses showed strong expression of *Helz2* mRNA in the liver, moderate expression in white adipose tissue (WAT) and brown adipose tissue (BAT), and very weak expression in the soleus muscle and hypothalamus (Figure 2, A and B). We then analyzed whether the expression of *Helz2* could be modulated by feeding conditions. qRT-PCR analyses revealed that fasting and refeeding states caused significant changes in hepatic *Helz2* mRNA expression, with the former increasing the expression and the latter reversing this increase. In contrast, no changes in *Helz2* mRNA expression were noted in WAT, BAT, the hypothalamus, or soleus muscle (Figure 2C). Moreover, chronic HFD feeding, which led to hepatosteatosis, elevated *Helz2* mRNA levels in the liver (Figure 2D) but not in other metabolic tissues of WT mice (data not shown). Because HFD feeding has been shown to up-regulate *Src-1* and *Src-2* expressions in adipocytes but not in other tissues, including the liver (32), the data together suggest that HFD feeding modifies the expression of different coregulators in tissue-specific manners. We also examined whether *HELZ2* mRNA levels could be altered in obese patients with nonalcoholic hepatosteatosis. Compared with control obese subjects without hepatosteatosis, the hepatic expression of *HELZ2* was significantly elevated in patients with hepatosteatosis (Figure 2E). These findings demonstrated that the expression of *Helz2* was up-regulated in the fatty liver of obese mice and human.

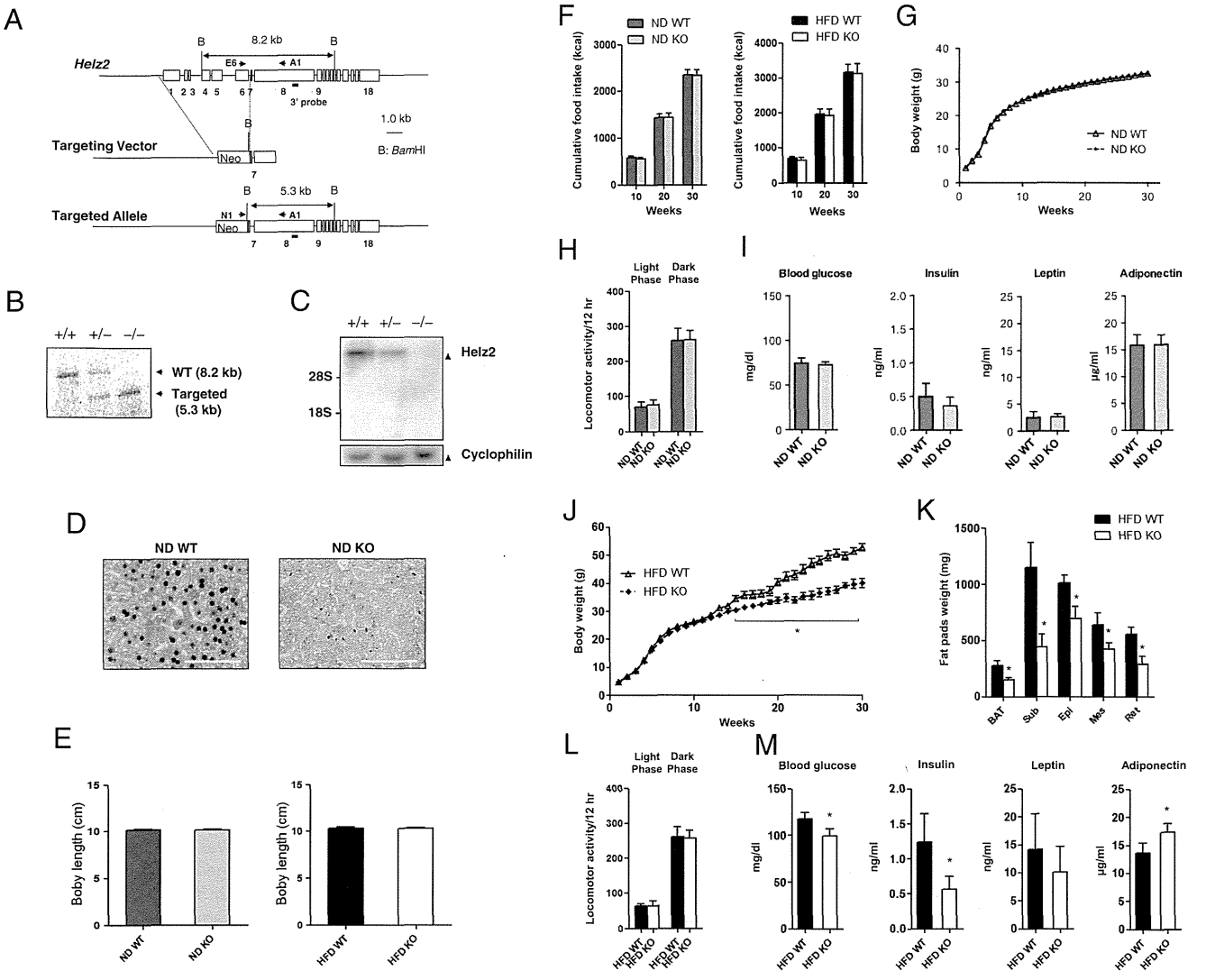

Figure 1. *Helz2*-deficient mice are protected against HFD-induced obesity. A, A targeting construct for generation of KO mice. A targeting vector substituting the NEO for exons 1–6 of the mouse *Helz2* gene was constructed to obtain KO mice. Positions of PCR primers for genotyping (E6, N1, and A1) and the probe for Southern blot analysis (3′ probe) are indicated with arrows and a bar, respectively. B, Germ line transmission of the modified *Helz2* allele. This was confirmed by Southern blot analysis of tail genomic DNA after *Bam*HI digestion. C, *Helz2* expression in the liver of KO mice. *Helz2* mRNA levels were quantitated by Northern blot analysis. Cyclophilin represents RNA loading reference. D, Immunohistochemistry for Helz2 in the liver. Abs were raised against several parts of the amino acid alignment of Helz2 protein. One (number 2–2332) of these Abs was used to determine the cellular localization of Helz2 in the liver. Photographs are representative of WT mice (left panel) and KO mice (right panel). Scale bars indicate 200 μm. E, Body length. Length from the top of the head to the end of the tail was measured in WT mice (left panel, n = 10) and KO mice (right panel, n = 10) fed either ND or HFD for 25 weeks. Data are the mean ± SEM. F, Cumulative food intake. Cumulative ND or HFD food intake is expressed as estimated kcal (n = 20 in each group). G, Changes in bw, which was measured in each mouse fed ND (n = 30–40 in each group). H, Locomotor activities of KO mice during light and dark phases. Locomotor activities were measured using an automatic counting manometer (n = 10 in each group). I, Blood levels of metabolic parameters in mice fed ND. Blood levels of glucose, insulin, leptin, and adiponectin were measured in mice fed ND for 25 weeks (n = 10 in each group). J, Changes in bw, which was measured in each mouse fed HFD (n = 30–40 in each group). K, Changes in fat deposition. Fat pad weights were measured in individual depots. Sub, sc fat; Epi, epididymal fat; Mes, mesenteric fat; Ret, retroperitoneal fat (n = 9 in each group). L, Locomotor activities of KO mice fed HFD during light and dark phases. Locomotor activities were measured using an automatic counting manometer (n = 10 in each group). M, Blood levels of metabolic parameters in mice fed HFD. Blood levels of glucose, insulin, leptin, and adiponectin were measured in mice fed HFD for 25 weeks (n = 10 in each group). WT, $Helz2^{+/+}$; KO, $Helz2^{-/-}$. Data are the mean ± SEM; *, $P < .05$ compared with WT mice.

Expression of Lepr in the liver, but not in the hypothalamus, was up-regulated in *Helz2* deficiency associated with central leptin resistance

Using cDNA microarray analyses, we next evaluated differences in hepatic gene expression profiles between HFD-fed WT and $Helz2^{-/-}$ mice. The alteration in the expression of the gene encoding *Lepr* was particularly pronounced, with up-regulation in $Helz2^{-/-}$ mice. We then examined time-dependent influences of *Helz2* deficiency on hepatic expression of the long form of Lepr (*Leprb*)

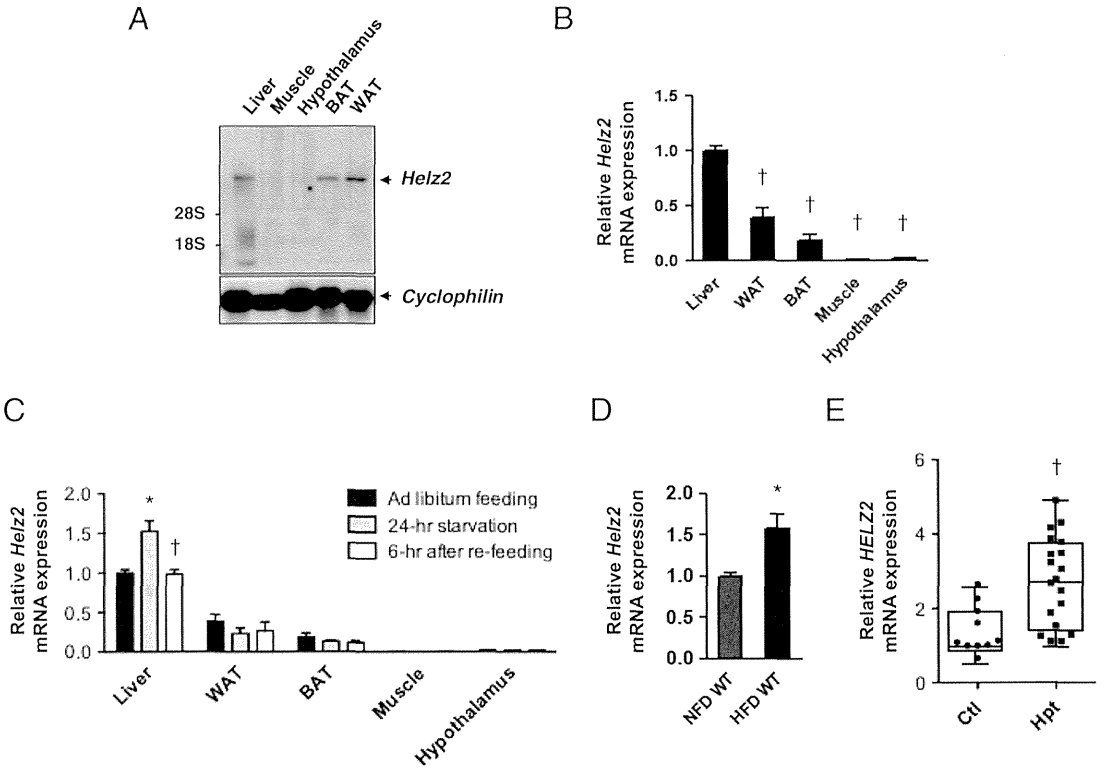

Figure 2. Expression of *Helz2* was up-regulated in fatty liver of mice and humans. A, Tissue expression of *Helz2*. Total RNAs isolated from individual tissue of WT mice were subjected to Northern blot analysis to determine *Helz2* mRNA expression using a ^{32}P-labeled *Helz2* cRNA probe. Cyclophilin (Cyclo) mRNA serves as an internal control for RNA loading. Positions of 28S and 18S ribosomal RNA are indicated. BAT, interscapular BAT; WAT, epididymal WAT. B, Tissue distribution of *Helz2* expression. *Helz2* expression was also measured by qRT-PCR in WT mice (n = 6 in each group) on ND. Data are shown as gene expression relative to those obtained in the liver of WT mice. †, $P < .05$ compared with the liver of WT mice fed ND. C, Effects of feeding states on *Helz2* expression in peripheral and hypothalamic tissues. *Helz2* expression was measured by qRT-PCR in WT mice fed ND ad libitum, fasted for 24 hours, and subsequently allowed to refeed for 6 hours. Data are shown as gene expression relative to that in the liver of mice fed ND ad libitum (n = 6 in each group). *, $P < .05$ compared with the ad libitum feeding group; †, $P < .05$ compared with the fasted group. D, *Helz2* expression in the liver of WT mice. *Helz2* expression was measured by qRT-PCR in liver samples of mice fed either ND or HFD for 25 weeks (n = 10 in each group). *, $P < .05$ compared with WT mice fed ND. E, *HELZ2* expression in the liver of patients with nonalcoholic fatty liver disease. *HELZ2* expression was measured by qRT-PCR in liver samples of control (Ctl) and hepatosteatosis (Hpt), as described in Materials and Methods. Data are shown as values relative to the Ctl (set at 1.0) and as box plots, in which boxes show the median and the 25th and 75th percentiles, and whiskers show the 10th and 90th percentiles. †, $P < .05$ compared with Ctl. Abbreviations are the same as those in Figure 1. Data are the mean ± SEM.

mRNA in HFD-fed mice: no change until 12 weeks of age, a 2-fold increase at 16 weeks, and a 5-fold increase at 25 weeks (Figure 3A). In contrast, levels of hepatic *Leprb* expression did not significantly differ between WT and *Helz2* KO mice on regular chow 8, 15, and 25 weeks after birth (Supplemental Figure 1). The hypothalamus, muscle, WAT, and BAT showed no alteration in *Leprb* expression on HFD (data not shown). In the liver of KO mice fed HFD, the short form of Lepr (*Lepra*) mRNA expression was also significantly increased (Figure 3B). Although the predicted molecular mass of Leprb is approximately 130 kDa, the glycosylated form of Leprb protein (~170 kDa) was observed in skeletal muscles by immunoblotting (33). As shown in Figure 3C, left panel, the predominant form of Leprb in the liver was approximately 170 kDa and the levels of hepatic Leprb in KO mice on HFD were significantly increased. In contrast, the major form of Leprb in the hypothalamus was approximately 130 kDa, and the levels of hypothalamic Leprb in KO mice did not differ from those in WT mice on HFD. As expected, approximately 130-kDa Leprb protein was not detected in the hypothalamus of *db/db* mice fed HFD, which lack functional Leprb because of a stop-codon mutation in exon 18b of the *Lepr* gene (Figure 3C, right panel) (34).

We next investigated whether liver-specific knockdown of *Helz2* influences hepatic *Leprb* mRNA levels in HFD-fed *Helz2*$^{+/+}$ mice by performing adenovirus-mediated transfer of shRNA directed toward *Helz2*. Twenty-four hours after tail-vein injection of shRNA, *Leprb* mRNA expression in the liver was increased but not in adipose tissues (Figure 3D). Moreover, repeated injection of adenovirus expressing shRNA significantly reduced HFD-induced bw gain (Figure 3E). These findings indicate that liver-specific knockdown of *Helz2* could directly enhance hepatic *Leprb* expression.

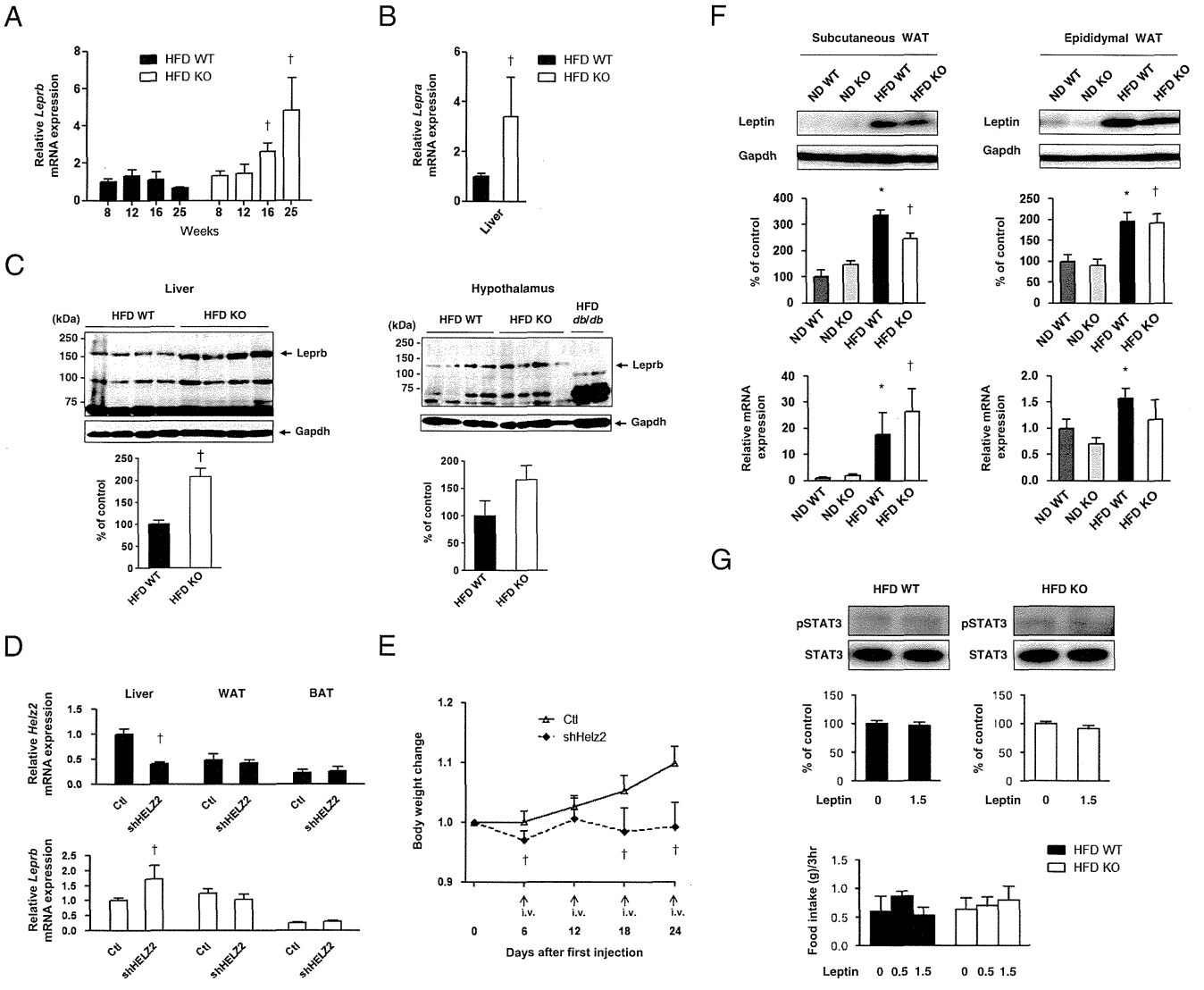

Figure 3. Expression of Lepr in the liver, but not in the hypothalamus, was up-regulated in *Helz2* deficiency associated with central leptin resistance. A, Chronological changes in hepatic *Leprb* expression after HFD feeding. WT and KO mice were fed HFD for 8–25 weeks, and hepatic *Leprb* expression was determined by qRT-PCR (n = 6 in each group). †, $P < .05$ compared with WT mice fed HFD at corresponding week. B, Changes in *Lepra* expression in liver. Mice were fed HFD for 25 weeks and hepatic *Lepra* expression was determined by qRT-PCR (n = 6 in each group). †, $P < .05$ compared with WT mice fed HFD. C, Changes in Leprb protein levels in the liver (left panel) and hypothalamus (right panel) of *Helz2* KO mice. Leprb was measured by immunoblotting of hepatic and hypothalamic proteins of WT and KO mice fed HFD for 25 weeks (n = 4 mice in each group). Hypothalamic protein of *db/db* mice fed HFD (n = 2) was immunoblotted in parallel. Representative immunoblots are shown above each graph. †, $P < .05$ compared with WT mice fed HFD. D, Effects of adenovirus-mediated *Helz2* knockdown on changes in *Helz2* and *Leprb* mRNA. HFD-fed WT mice received, at a 6-day interval, injection of either adenovirus-assisted shRNA (shHelz2) or control shRNA (Ctl). Six days after final injection, *Helz2* and *Leprb* mRNA were determined by qRT-PCR in the liver and other tissues. Data are shown as expression relative to those obtained in the livers of Ctl-injected mice. Each group comprised 6 mice. Data are the mean ± SEM; †, $P < .05$ compared with the Ctl-injected group. E, Changes in bws of HFD-fed WT mice receiving repeated administration of adenovirus-mediated *Helz2* knockdown. WT mice were given adenovirus-assisted shRNA targeting *Helz2*, or the Ctl at 6-day intervals. Data are shown as relative changes in bw gain from the start of injection. Each group comprised 6 mice. †, $P < .05$ compared with the Ctl-injected group. F, Leptin expression in adipocytes. Leptin protein and *Leptin* gene expression were determined by immunoblotting (middle panel) and qRT-PCR (bottom panel) in sc and epididymal WAT samples of WT and KO mice fed either ND or HFD. *, $P < .05$ and †, $P < .05$ compared with WT mice fed ND and HFD, respectively. Representative immunoblots are shown at the top. Each group comprised 6 samples. G, Changes in hypothalamic STAT3 phosphorylation and food intake after leptin administration in vivo. Each mouse (n = 5) fed HFD for 25 weeks received ip injection of leptin at a dose of 0, 0.5, or 1.5 μg/kg bw. pSTAT3 and total STAT3 in the hypothalamus were measured by immunoblotting 1 hour after injection (upper panels), and food intake was determined for 3 hours after injection (lower panels). Representative immunoblots are shown at the top. Abbreviations are the same as those in Figure 1. Data are the mean ± SEM.

Leptin activates STAT3 as a downstream signal in the hypothalamus (35). HFD-induced obesity is known to cause central leptin resistance showing blunted leptin-induced activation of hypothalamic STAT3 (36). As shown in Figures 1, I and M, and 3F, circulating serum leptin levels and adipose *Leptin* mRNA and protein expression

were significantly higher in HFD-fed WT and KO mice than in ND-fed WT and KO mice. Hypothalamic Leprb mRNA, protein levels, and food intake were unaffected by *Helz2* deficiency (Figures 1F and 3C and data not shown), implying little influence of *Helz2* deficiency on the hypothalamus, probably because of its low hypothalamic expression. Indeed, ip injections of leptin neither activated hypothalamic STAT3 nor suppressed food intake in HFD-fed *Helz2*$^{-/-}$ mice (Figure 3G) in contrast to ND-fed WT and KO mice (Supplemental Figure 2). These findings suggest that HFD-fed *Helz2* KO mice showed central leptin resistance in association with liver-specific increased expression of Leprb.

Increased hepatic expression of *Leprb* activates AMPK on HFD

It is known that leptin activates AMPK as a downstream signal in the liver and muscle (37, 38), and hepatic deficiency of AMPK diminishes leptin-induced metabolic actions in the liver (39). Hepatic AMPK activation is reported to be blunted in obese patients (40), and reduced expression of *Lepr* in the liver was observed in obese patients (41). As shown in Figure 4, A and B, pAMPK and its target molecule, ACC, were increased in the liver, but not in the muscle, of HFD-fed *Helz2*$^{-/-}$ mice. Adenovirus-mediated *Helz2* knockdown by shRNA could also activate hepatic AMPK (Figure 4C). Moreover, leptin treatment apparently augmented AMPK phosphorylation in primary hepatocytes prepared from HFD-fed *Helz2*$^{-/-}$ mice (Figure 4D). These data together provide evidence that the liver with increased Leprb expression in *Helz2* KO mice is sensitive to endogenous or exogenously administered leptin followed by AMPK activation.

To next clarify whether liver-specific Leprb up-regulation is essential to activate hepatic AMPK under HFD conditions, we evaluated the direct effects of repeated injection, at 6-day intervals, of adenovirus-mediated exogenous Leprb overexpression on AMPK activation in HFD-fed WT mice with low hepatic Leprb expression. Adenovirus-mediated Leprb overexpression produced a significant increase in *Leprb* mRNA (Figure 4E) and protein levels (Supplemental Figure 3) followed by significant AMPK activation in the liver (Figure 4F). In adipose tissues, no significant changes in *Leprb* expression were observed after adenoviral injection (Figure 4E). Consequently, hyperlipidemia and bw gain were significantly attenuated by liver-specific Leprb overexpression in HFD-fed WT mice (Figure 4, G and H), although food intake was not altered in these mice (Figure 4I). These findings provide additional evidence that the increased expression of hepatic Leprb plays important roles to protect against HFD-induced bw gain and dyslipidemia by stimulating AMPK in the liver.

Hepatic *Leprb* is essential to activate AMPK in *Helz2* KO mice on HFD

To further address whether hepatic Leprb overexpression caused by *Helz2* deficiency is essential to activate AMPK in vivo, *Helz2* KO mice were crossed with *db/db* mice. In immunoblot analyses, established *Helz2*-deficent *db/db* mutants showed no expression of hepatic Leprb, and levels of pAMPK in the liver of these mutants were indistinguishable from those in *Helz2*$^{+/+}$*/db/db* mice (Figure 5, A and B). In addition, leptin treatment did not increase pAMPK in primary hepatocytes derived from double mutant mice (Figure 5C), indicating that functional Leprb was essential for leptin-induced hepatic AMPK activation. Subsequently, *Helz2*$^{-/-}$*db/db* mice were not protected against obesity (Figure 5D).

Hepatic lipogenesis is attenuated and hepatic FA oxidation is increased in *Helz2* KO mice fed HFD

The PPAR family consists of 3 subfamily members, PPARα, PPARδ, and PPARγ, and each PPAR isotype shows different functions for hepatic lipid metabolism (42). Helz2 functions as a coactivator of PPARγ in vitro (21, 22) but is not involved in hepatic fat accumulation mediated by adenovirally overexpressed PPARγ in vivo (43). In conjunction with PPARα, PPARδ and PGC-1α, the AMPK energy-sensing pathway regulates hepatic metabolic function (37, 44, 45). AMPK stimulates transcription of these genes under conditions in which these molecules are not phosphorylated (46–48). The expression of *Pparα*, *Pparδ*, and *Pgc-1α*, but not *Pparγ*, *Src-1*, *Src-2*, or *Cbp*, was increased in the liver of *Helz2* KO mice on HFD (Figure 6A).

HFD-induced hepatic lipogenesis augments the accumulation of intrahepatic TG, resulting in hepatosteatosis, which can develop independently of increased visceral adiposity and contributes to metabolic dysfunction (42, 49). PPARα and PPARδ regulate the transcription of various target genes involved in hepatic metabolism (37, 44, 45), particularly PGC-1α, which significantly participates in regulating lipogenesis rather than gluconeogenesis in the liver (50). Among the lipogenic genes examined (Figure 6B), *Helz2* deficiency decreased the expression of the gene encoding stearoyl-coenzyme A desaturase-1 (*Scd1*), a rate-limiting enzyme producing monounsaturated FA, whose expression is known to be decreased by leptin (51). *Helz2* deficiency also reduced expression of the genes encoding 1-acylglycerol-3-phosphate O-acyltransferase-2 (*Agpat2*) and monoacylglycerol O-acyltransferase-1 (*Mgat1*), which are important for lipid synthesis (52). Consequently, hyperlipidemia was ameliorated in *Helz2*$^{-/-}$ mice (Figure 6C). In contrast, hepatic expression of these lipogenic and FA oxidation-related genes or serum lipid levels was not altered *Helz2*-deficent *db/db* mutants (Figure 6, D and E, and Supplemental Figure 4).

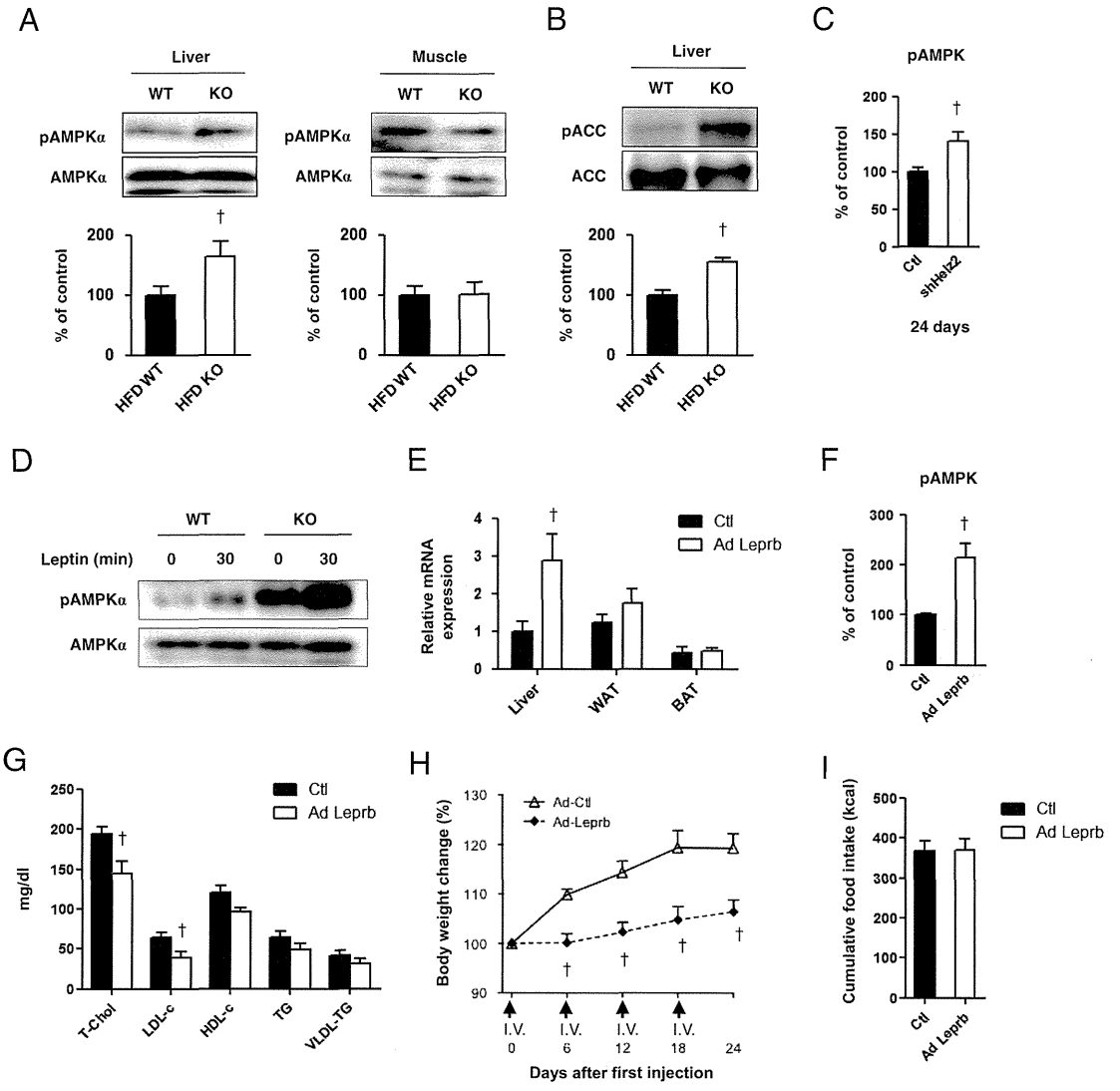

Figure 4. Increased hepatic expression of *Leprb* activates AMPK in *Helz2* KO mice on HFD. A, AMPK phosphorylation in the liver and soleus muscle. pAMPK and total AMPK were measured by immunoblotting proteins from the liver (left panel) and muscle (right panel) of mice fed HFD for 25 weeks. Representative immunoblots are shown above each graph (n = 6 in each group). B, ACC phosphorylation in the liver. pACC and total ACC was measured by immunoblotting liver proteins of mice fed HFD. Representative immunoblots are shown above each graph (n = 6 in each group). C, Effects of adenovirus-mediated *Helz2* knockdown on AMPK activation in the liver. The groups were the same as those in Figure 3D. Twenty-four days after injection, liver samples were determined for pAMPK using an AMPK (pT172) ELISA kit (Invitrogen). Each group comprised 6 samples. D, In vitro leptin-induced AMPK phosphorylation in primary hepatocytes. Hepatocytes isolated from mice fed HFD for 25 weeks were incubated with leptin (10nM) for 30 minutes. AMPK phosphorylation was measured by immunoblotting. A representative immunoblot from 3 individual experiments with similar results is shown. E, Effects of adenovirus-mediated *Leprb* overexpression on *Leprb* expression in the liver. HFD-fed WT mice received repeated tail-vein injection of either the adenovirus-assisted *Leprb* expression (Ad-Leprb) or the control adenovirus (Ad-Ctl). Six days after injection, *Leprb* mRNA was determined by qRT-PCR of the liver, WAT and BAT. Data are shown as expressions relative to those obtained in the liver of mice with Ctl injection. Each group comprised 5 mice. F, Effects of adenovirus-mediated *Leprb* overexpression on AMPK activation in the liver of HFD-fed WT mice receiving adenovirus-mediated *Leprb* overexpression. Liver samples were determined for pAMPK by an AMPK (pT172) ELISA kit. Each group comprised 5 samples. G, Changes in the blood lipid profiles in HFD-fed WT mice receiving repeated administration of adenovirus-mediated *Leprb* overexpression. Mice (n = 5) were given repeated injections of adenovirus at 6-day intervals, and blood lipid levels were determined after the final injection. H, Effects of adenovirus-mediated *Leprb* overexpression on bw gain during a 24-day period. The groups were the same as those described in Figure 4E. Body weight gains are expressed as relative changes from the bws before adenovirus injection (n = 5 in each group). I, Food intake in mice receiving adenovirus-mediated *Leprb* overexpression (Ad-Leprb). Cumulative HFD intake during 24 days is expressed as estimated kcal. Each group comprised 5 mice. Abbreviations are the same as those in Figure 1. Data are the mean ± SEM; †, $P < .05$ compared with WT mice fed HFD or Ctl-injected group, respectively.

Activated AMPK influences hepatic FA oxidation (36, 37). In *Helz2* KO mice, hepatic AMPK activation elevated the expression of genes encoding carnitine palmitoyltransferase-1a (*Cpta1*) and long-chain-acyl-coenzymeA dehydrogenase (*Lcad*), key enzymes for FA-β oxidation in mitochondria (53). The expression of *Cyp4a10*, a mole-

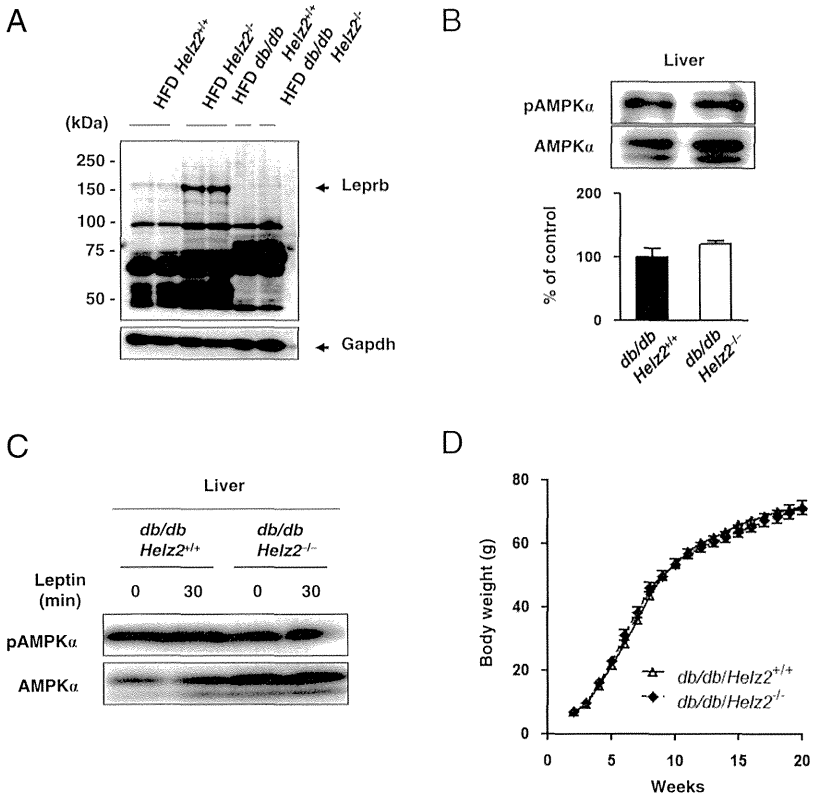

Figure 5. Hepatic *Leprb* is essential to activate AMPK in *Helz2* KO mice on HFD. A, Leprb protein expression in the liver of *Helz2*-deficient *db/db* mice. Leprb expression was measured by immunoblotting hepatic proteins of mutated mice fed HFD for 20 weeks. Images are representative of 2 individual experiments. B, Hepatic AMPK phosphorylation in *Helz2*-deficient *db/db* mice. AMPK phosphorylation was measured by Western blotting the liver proteins of mutated mice fed HFD for 20 weeks (n = 5 in each group). C, In vitro leptin-induced AMPK phosphorylation in primary hepatocytes of *Helz2*-deficient *db/db* mice. Hepatocytes isolated from *Helz2*$^{+/+}$*db/db* and *Helz2*$^{-/-}$*db/db* mice fed HFD were incubated with leptin (10nM) for 30 minutes. AMPK phosphorylation was measured by immunoblotting. Images are representative of 2 individual experiments. D, Changes in bw gain in *Helz2*-deficient *db/db* mice. Each group comprised 20 mice. Abbreviations are the same as those in Figure 1. Data are the mean ± SEM.

cule involved in microsomal FA-ω oxidation, was also increased (Figure 6F). In a consistent manner, ^{14}C-palmitate oxidation was significantly increased in the liver of *Helz2* KO mice, but not in the muscle, under HFD conditions (Figure 6G).

The expression of FA oxidation-controlling genes should be elevated when adipocytes have high Leprb expression, which subsequently causes hyperthermia (54), but these gene expressions were not elevated in WAT or BAT of HFD-fed *Helz2*$^{-/-}$ mice (Figure 6F), whose body temperature remained unchanged (Figure 6H). Because metaboloregulatory thermogenesis occurs in BAT and WAT showing increased FA oxidation under ambient conditions (55), the data suggest that energy dissipated in BAT and WAT does not explain obesity protection in *Helz2*-deficient mice on HFD. VO_2 was increased and RQ was lowered in HFD-fed *Helz2*$^{-/-}$ mice compared with *Helz2*$^{+/+}$ mice, and these parameters were identical in the 2 ND-fed groups (Figure 6I). Taken together, increased FA oxidation in the liver could play critical roles in the protection against HFD-induced bw gain.

Hepatosteatosis and insulin resistance are improved in *Helz2*$^{-/-}$ mice on HFD

Obese *Helz2*$^{+/+}$ mice on HFD show insulin resistance (Figure 1M). *Helz2* deficiency on HFD significantly reduced hepatic enlargement and TG content and ameliorated histological findings of hepatosteatosis (Figure 7A). Moreover, insulin-induced hepatic Akt activation in vitro and insulin sensitivity in vivo were apparently increased in HFD-fed *Helz2*$^{-/-}$ mice (Figure 7, B and C), which consequently ameliorated glucose intolerance (Figure 7D).

Discussion

The state of leptin resistance involves the development of tissue-specific failure of leptin signaling (10, 11). Molecular mechanisms underlying central leptin resistance associated with overweight and obesity have been studied extensively, and diverse molecules involved in leptin transport, Leprb signaling, and leptin-targeted neural circuits have been implicated in the development of central leptin resistance (11, 56). The present study demonstrates that *Helz2* deficiency does not promote Leprb overexpression or suppressor of cytokine signaling 3 reduced expression in the hypothalamus and that serum leptin levels are indistinguishably elevated between *Helz2*-deficient mice and WT mice on HFD. Moreover, endogenously or exogenously administered leptin failed to activate hypothalamic STAT3 or reduce food intake in both mice. These findings together suggest the presence of apparent central leptin resistance in *Helz2*-deficient mice, similar to WT mice. In spite of central resistance to leptin, *Helz2* KO mice are exclusively protected against HFD-induced obesity.

In the present study, mice fed HFD and obese patients with hepatosteatosis showed significantly increased expression of *Helz2*, leading to suppression of the expression

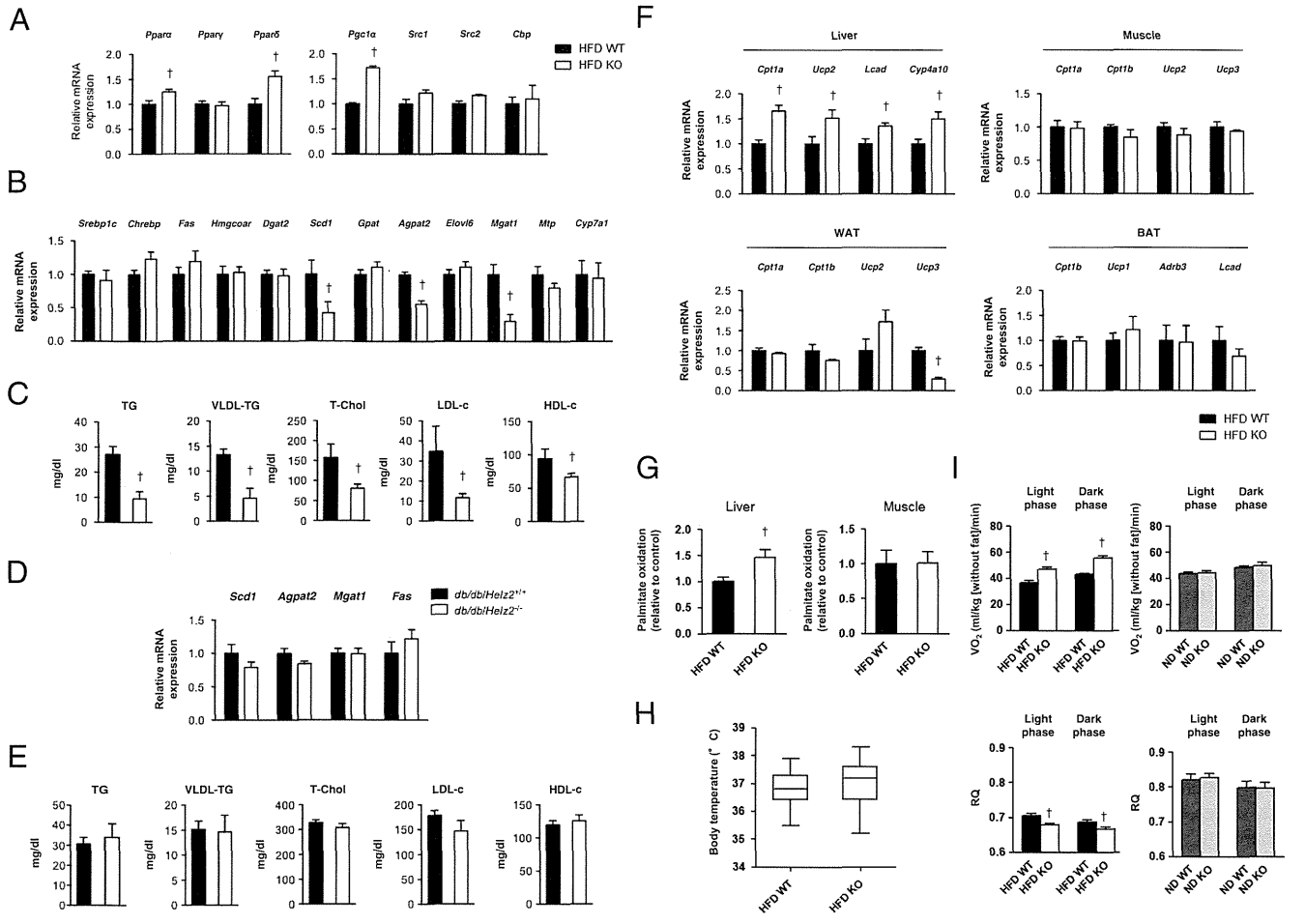

Figure 6. Hepatic lipogenesis is attenuated and hepatic FA oxidation (FAO) is increased in *Helz2* KO mice fed HFD. A, Changes in the gene expression of PPARs and coregulators in the liver. Expressions of indicated genes in the liver were quantitated by qRT-PCR in mice fed HFD for 25 weeks (n = 6 in each group). B, Hepatic lipogenesis gene expression in *Helz2* KO mice. Hepatic expression of the genes controlling lipogenesis was determined in *Helz2* KO mice fed HFD for 25 weeks. Each expression of the indicated genes in the liver was evaluated by qRT-PCR (n = 6 in each group). C, Changes in the blood lipid profiles. Serum lipid profiles in mice fed HFD for 25 weeks were analyzed (n = 10 in each group). T-Chol, total cholesterol; LDL-c, low-density-lipoprotein cholesterol; HDL-c, high-density-lipoprotein cholesterol; VLDL-TG, very-LDL TG. D, Hepatic lipogenesis gene expression in *Helz2*-deficient *db/db* mice. Hepatic expressions of the genes controlling lipogenesis were determined in *Helz2*$^{+/+}$*db/db* and *Helz2*$^{-/-}$*db/db* mice fed HFD (n = 6 in each group). E, Blood lipid levels in *Helz2*-deficient *db/db* mice. Blood lipid levels were determined in *Helz2*$^{+/+}$*db/db* and *Helz2*$^{-/-}$*db/db* mice fed HFD for 20 weeks (n = 6 in each group). F, FAO-associated gene expression in peripheral tissues. Expressions of indicated genes were measured by qRT-PCR in the liver, soleus muscle, WAT, and BAT of mice fed HFD (n = 6 in each group). G, Measurement of FAO in the liver and muscle of *Helz2* KO mice. FAO was evaluated in the liver and muscle of mice fed for 25 weeks, as described in Materials and Methods (n = 7 in each group). H, Body temperature. Using a thermometer, core temperature was measured at room temperature (24°C) in WT mice and KO mice fed HFD for 25 weeks. Each group comprised 10 mice. Data are shown as box-and-whisker plots. I, Changes in VO_2 and RQ. VO_2 (upper panel) and RQ (lower panel) were measured in mice fed HFD or ND for 25 weeks. Data are expressed as values to bws excluding fat mass (n = 7 in each group). Abbreviations are the same as those in Figure 1. Data are the mean ± SEM; †, $P < .05$ compared with WT mice fed HFD, respectively.

of *Leprb* in the liver. On the other hand, *Helz2* deficiency under HFD conditions significantly increased hepatic expression of endogenous *Leprb* in a tissue-specific manner. Marked hyperleptinemia, together with increased *Leprb* expression in *Helz2*-deficient mice, apparently contributes to AMPK activation in the liver. Notably, in vitro leptin administration directly augmented AMPK phosphorylation in primary hepatocytes prepared from HFD-fed KO mice. Activated AMPK, in turn, suppressed lipogenesis and stimulated FA oxidation in the liver by altering the expression of genes involved in hepatic lipid metabolism. Analogous to these observations, adenovirally mediated liver-specific *Leprb* overexpression in HFD-fed WT mice with low hepatic *Leprb* expression resulted in significant AMPK activation, and HFD-induced hyperlipidemia and bw gain improved in these mice without altering food intake. In contrast, the liver of *Helz2*-deficient *db/db* mice showed neither Leprb expression nor AMPK activation, and in vitro treatment with leptin did not activate AMPK in hepatocytes derived from these mice. Accord-

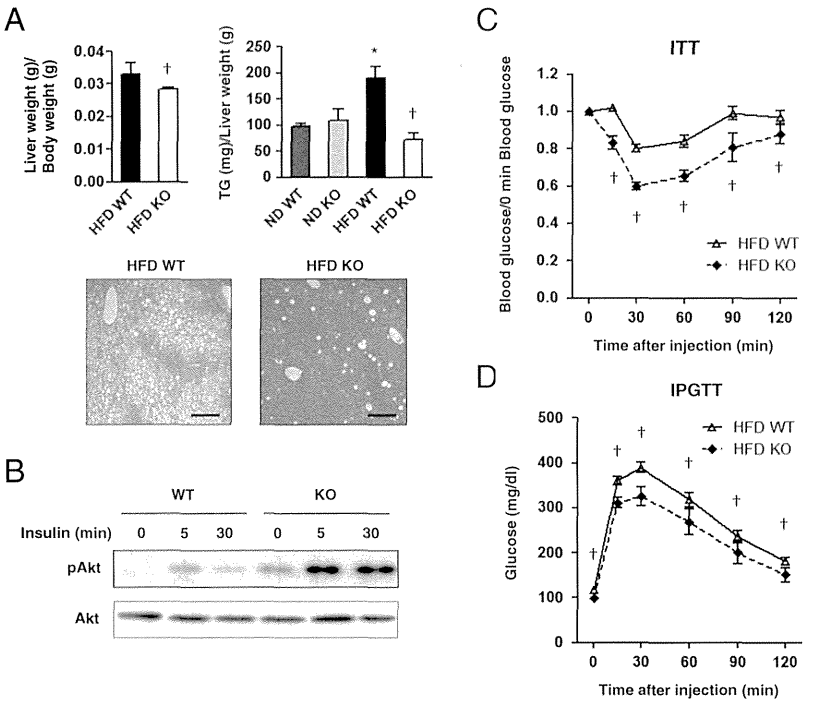

Figure 7. Hepatosteatosis and insulin resistance are improved in *Helz2*$^{-/-}$ mice on HFD. A, Changes in liver weights and hepatic TG contents. Liver weights (left upper panel) and hepatic TG contents (right upper panel) of mice fed HFD for 25 weeks were measured (n = 10 in each group). Representative pictures of liver sections stained with HE of WT and KO mice fed HFD are shown. Scale bar indicates 200 μm. B, Insulin-induced Akt phosphorylation in primary hepatocytes. Hepatocytes prepared from WT and KO mice fed HFD were incubated with insulin (100nM) for 5 and 30 minutes. pAkt and total Akt were measured by immunoblotting. A representative immunoblot from 3 individual experiments is shown. C, Insulin sensitivity in mice fed HFD. The insulin tolerance test (ITT) was performed in WT and KO mice fed HFD for 25 weeks by ip injection of regular insulin (0.5 U/kg bw). Subsequent blood samples were used to determine blood glucose levels. Data are shown as relative changes from levels before insulin injection (n = 10 in each group). D, Glucose intolerance. WT and KO mice fed HFD for 25 weeks received ip injection of glucose (1.0 g glucose/kg bw). Blood samples were drawn at the indicated times, and glucose levels were measured. Each group comprised 10 mice. Abbreviations are the same as those in Figure 1. Data are the mean ± SEM; *, $P < .05$ and †, $P < .05$ compared with WT mice fed ND and HFD, respectively.

ingly, the improvement of hyperlipidemia and reduction of bw gain observed in *Helz2*-deficient mice on HFD were completely lost in these double KO mice. AMPK activation induced by *Helz2* deficiency eventually resulted in apparent amelioration of hepatosteatosis and insulin resistance under HFD conditions. HFD-fed *Helz2* KO mice revealed neither *Leprb* overexpression nor stimulation of FA oxidation in skeletal muscle, WAT, or BAT (Figure 6G and data not shown), and their locomotor activities as well as body temperature remained unchanged. Thus, energy expenditure in these metabolic tissues was not responsible for the antiobesity effects of *Helz2* deficiency. Taken together, these findings suggest the intriguing possibility that whole-body metabolic abnormalities could be ameliorated by enhanced peripheral leptin sensitivity through the activation of endogenous *Leprb* expression in the liver, independently of central leptin resistance. Nonetheless, because *Helz2* is expressed in the hypothalamus at low levels, we could not rule out the possibility that deletion of *Helz2* in the central nervous system might in part influence the metabolic phenotype of Helz2 KO mice on HFD. In addition, further study is required to elucidate the molecular mechanism of how Helz2 regulates hepatic Leprb expression.

To date, a number of KO mouse models of PPARγ coregulators, including Cbp, Mediator complex subunit 1, Src-1, Src-2, Src-3, and Pgc-1α have been generated and their metabolic phenotypes intensively analyzed (19, 20). Despite apparent lipodystrophy caused by impaired transcriptional activities of PPARγ and CCAAT/enhancer binding protein β, *Cbp*$^{+/-}$ mice are insulin sensitized and resistant to HFD-induced obesity due to reduced hepatic lipogenesis and increased FA oxidation in the liver and muscle in association with the increased secretion of leptin and adiponectin (57). Liver-specific *Med1* inactivation consistently inhibits hepatic PPARα and PPARγ signaling and the development of HFD-induced fatty liver (43, 58). Mice lacking *Src-1* are prone to obesity as a result of their reduced capacity for energy expenditure and FA oxidation in BAT (32). The inactivation of *Src-2* in mice resulted in a lean phenotype that correlates with the decreased expression of genes involved in the uptake and storage of FAs and with increased lipolysis on ND (32). As expected from the highest expression of *Src-3* in WAT, *Src3*$^{-/-}$ mice revealed reduced bw and adipose tissue mass with a significant decrease of the expression of adipogenic genes on ND (59). *Pgc-1*α null mice are lean and resistant to HFD-induced obesity, largely due to profound hyperactivity, which is controlled by the striatal region in the brain (60). These accumulated data and the present findings collectively suggest that the characteristic phenotypes induced by general knockout of endogenous coregulators could occur largely depending on the different magnitude of their original tissue expression. Moreover, the global impact of coregulators on whole-body energy homeostasis could de-

pend on their capacity to modulate metabolic balance by promoting or inhibiting anabolic and catabolic functions.

From the clinical aspect, leptin replacement therapy for lipodystrophy patients showing hypoleptinemia successfully improved lipid and glucose metabolisms. However, leptin monotherapy failed to ameliorate metabolic abnormalities in obese patients showing hyperleptinemia associated with central leptin resistance (11, 56). The present findings suggest that hepatic HELZ2 could be a novel target molecule for the treatment of obese patients with central leptin resistance.

Acknowledgments

We thank A. Miura, Y. Ariyama, H. Yamada, M. Murakami, and Y. Kitamura (Gunma University) for their technical assistance and thank Dr Y. Rouillé (Institut Pasteur de Lille) for providing the expression plasmid of Leprb.

Address all correspondence and requests for reprints to: Tetsurou Satoh, MD, PhD, Department of Medicine and Molecular Science, Gunma University Graduate School of Medicine, Showa-machi, Maebashi 371–8511, Japan. E-mail: tsato@gunma-u.ac.jp.

This work was supported by Grants-in-Aid from the Ministry of Science, Education, Sports and Culture of Japan, Takeda Science Foundation, Naito Foundation of Japan, the Joint Research Program of the Institute for Molecular and Cellular Regulation, Gunma University, and the Global Center of Excellence Program of Japan (Ma.Mori and T.Sat.).

Disclosure Summary: The authors have nothing to disclose.

References

1. **Wang YC, McPherson K, Marsh T, Gortmaker SL, Brown M.** Health and economic burden of the projected obesity trends in the USA and the UK. *Lancet.* 2011;378:815–825.
2. **Shimizu H, Inoue K, Mori M.** The leptin-dependent and -independent melanocortin signaling system: regulation of feeding and energy expenditure. *J Endocrinol.* 2007;193:1–9.
3. **Rothwell NJ, Stock MJ.** Regulation of energy balance. *Ann Rev Nutr.* 1981;1:235–256.
4. **Cannon B, Nedergaard J.** Brown adipose tissue: function and physiological significance. *Physiol Rev.* 2004;84:277–359.
5. **Flier JS.** Obesity wars: molecular progress confronts an expanding epidemic. *Cell.* 2004;116:337–350.
6. **Zhang Y, Proenca R, Maffei M, Barone M, Leopold L, Friedman JM.** Positional cloning of the mouse obese gene and its human homologue. *Nature.* 1994;372:425–432.
7. **Cottrell EC, Mercer JG.** Leptin receptors. *Handb Exp Pharmacol.* 2012;209:3–21.
8. **Muoio DM, Lynis Dohm G.** Peripheral metabolic actions of leptin. *Best Pract Res Clin Endocrinol Metab.* 2002;16:653–666.
9. **Huang W, Dedousis N, Bandi A, Lopaschuk GD, O'Doherty RM.** Liver triglyceride secretion and lipid oxidative metabolism are rapidly altered by leptin in vivo. *Endocrinology.* 2006;147:1480–1487.
10. **Shimizu H, Oh-I S, Okada S, Mori M.** Leptin resistance and obesity. *Endocr J.* 2007;54:17–26.
11. **Myers MG Jr, Heymsfield SB, Haft C, et al.** Challenges and opportunities of defining clinical leptin resistance. *Cell Metab.* 2012;15:150–156.
12. **Pihlajamäki J, Boes T, Kim EY, et al.** Thyroid hormone-related regulation of gene expression in human fatty liver. *J Clin Endocrinol Metab.* 2009;94:3521–3529.
13. **Cohen P, Zhao C, Cai X, et al.** Selective deletion of leptin receptor in neurons leads to obesity. *J Clin Invest.* 2001;108:1113–1121.
14. **Baskin DG, Seeley RJ, Kuijper JL, et al.** Increased expression of mRNA for the long form of the leptin receptor in the hypothalamus is associated with leptin hypersensitivity and fasting. *Diabetes.* 1998;47:538–543.
15. **Lee Y, Wang MY, Kakuma T, et al.** Liporegulation in diet-induced obesity. The antisteatotic role of hyerleptinemia. *J Biol Chem.* 2001;276:5629–5635.
16. **Tontonoz P, Hu E, Graves RA, Budavari AI, Spiegelman BM.** mPPARγ2: tissue-specific regulator of an adipocyte enhancer. *Genes Dev.* 1994;8:1224–1234.
17. **Rosen ED, Sarraf P, Troy AE, et al.** PPAR γ is required for the differentiation of adipose tissue in vivo and in vitro. *Mol Cell.* 1999;4:611–617.
18. **Lehrke M, Lazar MA.** The many faces of PPARγ. *Cell.* 2005;123:993–999.
19. **Feige JN, Auwerx J.** Transcriptional coregulators in the control of energy homeostasis. *Trends Cell Biol.* 2007;17:292–301.
20. **Lonard DM, O'Malley BW.** Nuclear receptor coregulators: modulators of pathology and therapeutic targets. *Nat Rev Endocrinol.* 2012;8:598–604.
21. **Tomaru T, Satoh T, Yoshino S, et al.** Isolation and characterization of a transcriptional cofactor and its novel isoform that binds the deoxyribonucleic acid-binding domain of peroxisome proliferator-activated receptor-γ. *Endocrinology.* 2006;147:377–388.
22. **Surapureddi S, Yu S, Bu H, et al.** Identification of α transcriptionally active peroxisome proliferator-activated receptor α-interacting cofactor complex in rat liver and characterization of PRIC285 as a coactivator. *Proc Natl Acad Sci USA.* 2002;99:11836–11841.
23. **Altamura N, Groudinsky O, Dujardin G, Slonimski PP.** NAM7 nuclear gene encodes a novel member of a family of helicases with a Zn-ligand motif and is involved in mitochondrial functions in *Saccharomyces cerevisiae*. *J Mol Biol.* 1992;224:575–587.
24. **Kang YH, Lee CH, Seo YS.** Dna2 on the road to Okazaki fragment processing and genome stability in eukaryotes. *Crit Rev Biochem Mol Biol.* 2010;45:71–96.
25. **Katano-Toki A, Satoh T, Tomaru T, et al.** THRAP3 interacts with HELZ2 and plays a novel role in adipocyte differentiation. *Mol Endocrinol.* 2013;27:769–780.
26. **Anai M, Funaki M, Ogihara T, et al.** Enhanced insulin-stimulated activation of phosphatidylinositol 3-kinase in the liver of high-fat-fed rats. *Diabetes.* 1999;48:158–169.
27. **Oh-I S, Shimizu H, Satoh T, et al.** Identification of nesfatin-1 as a satiety molecule in the hypothalamus. *Nature.* 2006;443:709–712.
28. **Folch J, Lees M, Sloane Stanley GH.** A simple method for the isolation and purification of total lipides from animal tissues. *J Biol Chem.* 1957;226:497–509.
29. **Mori M, Murata Y, Kotani T, et al.** Promotion of cell spreading and migration by vascular endothelial-protein tyrosine phosphatase (VE-PTP) in cooperation with integrins. *J Cell Physiol.* 2010;224:195–204.
30. **Sasaki T, Kim HJ, Kobayashi M, et al.** Induction of hypothalamic Sirt1 leads to cessation of feeding via agouti-related peptide. *Endocrinology.* 2010;151:2556–2566.
31. **Izumiya Y, Hopkins T, Morris C, et al.** Fast/glycolytic muscle fiber growth reduces fat mass and improves metabolic parameters in obese mice. *Cell Metab.* 2008;7:159–172.
32. **Picard F, Géhin M, Annicotte J, et al.** SRC-1 and TIF2 control energy balance between white and brown adipose tissues. *Cell.* 2002;111:931–941.

33. **Fuentes T, Ara I, Guadalupe-Grau A, et al.** Leptin receptor 170 kDa (Ob-R170) protein expression is reduced in obese human skeletal muscle: a potential mechanism of leptin resistance. *Exp Physiol.* 2010;95:160–171.
34. **Chen H, Charlat O, Tartaglia LA, et al.** Evidence that the diabetes gene encodes the leptin receptor: identification of a mutation in the leptin receptor gene in *db/db* mice. *Cell.* 1996;84:491–495.
35. **Bates SH, Stearns WH, Dundon TA, et al.** STAT3 signalling is required for leptin regulation of energy balance but not reproduction. *Nature.* 2003;421:856–859.
36. **Bjørbaek C, Elmquist JK, Frantz JD, Shoelson SE, Flier JS.** Identification of SOCS-3 as a potential mediator of central leptin resistance. *Mol Cell.* 1998;1:619–625.
37. **Kahn BB, Alquier T, Carling D, Hardie DG.** AMP-activated protein kinase: ancient energy gauge provides clues to modern understanding of metabolism. *Cell Metab.* 2005;1:15–25.
38. **Zhang BB, Zhou G, Li C.** AMPK: an emerging drug target for diabetes and the metabolic syndrome. *Cell Metab.* 2009;9:407–416.
39. **Andreelli F, Foretz M, Knauf C, et al.** Liver adenosine monophosphate-activated kinase-α2 catalytic subunit is a key target for the control of hepatic glucose production by adiponectin and leptin but not insulin. *Endocrinology.* 2006;147:2432–2441.
40. **Brabant G, Müller G, Horn R, Anderwald C, Roden M, Nave H.** Hepatic leptin signaling in obesity. *FASEB J.* 2005;19:1048–1050.
41. **Elam MB, Cowan GS Jr, Rooney RJ, et al.** Hepatic gene expression in morbidly obese women: implications for disease susceptibility. *Obesity.* 2009;17:1563–1573.
42. **Reddy JK, Rao MS.** Lipid metabolism and liver inflammation. II. Fatty liver disease and fatty acid oxidation. *Am J Physiol Gastrointest Liver Physiol.* 2006;290:G852–G858.
43. **Bai L, Jia Y, Viswakarma N, et al.** Transcription coactivator mediator subunit MED1 is required for the development of fatty liver in the mouse. *Hepatology.* 2011;53:1164–1174.
44. **Patsouris D, Reddy JK, Müller M, Kersten S.** Peroxisome proliferator-activated receptor α mediates the effects of high-fat diet on hepatic gene expression. *Endocrinology.* 2006;147:1508–1516.
45. **Røst TH, Haugan Moi LL, Berge K, Staels B, Mellgren G, Berge RK.** A pan-PPAR ligand induces hepatic fatty acid oxidation in PPARα-/- mice possibly through PGC-1 mediated PPARδ coactivation. *Biochim Biophys Acta.* 2009;1791:1076–1083.
46. **Suzuki A, Okamoto S, Lee S, Saito K, Shiuchi T, Minokoshi Y.** Leptin stimulates fatty acid oxidation and peroxisome proliferator-activated receptor α gene expression in mouse C2C12 myoblasts by changing the subcellular localization of the α2 form of AMP-activated protein kinase. *Mol Cell Biol.* 2007;27:4317–4327.
47. **Irrcher I, Ljubicic V, Kirwan AF, Hood DA.** AMP-activated protein kinase-regulated activation of the PGC-1α promoter in skeletal muscle cells. *PLoS One.* 2008;3:e3614:1–10.
48. **Narkar VA, Downes M, Yu RT, et al.** AMPK and PPAR-δ agonists are exercise mimetics. *Cell.* 1008;134:405–415.
49. **Williams KH, Shackel NA, Gorrell MD, McLennan SV, Twigg SM.** Diabetes and nonalcoholic fatty liver disease: a pathogenic duo. *Endocrine Rev.* 2013;34:84–129.
50. **Estall JL, Kahn M, Cooper MP, et al.** Sensitivity of lipid metabolism and insulin signaling to genetic alterations in hepatic peroxisome proliferator-activated receptor-γ coactivator-1α expression. *Diabetes.* 2009;58:1499–1508.
51. **Cohen P, Miyazaki M, Socci ND, et al.** Role for stearoyl-CoA desaturase-1 in leptin-mediated weight loss. *Science.* 2002;297:240–343.
52. **Cortés VA, Curtis DE, Sukumaran S, et al.** Molecular mechanisms of hepatic steatosis and insulin resistance in the AGPAT2-deficient mouse model of congenital generalized lipodystrophy. *Cell Metab.* 2009;9:165–176.
53. **Zhang D, Liu ZX, Choi CS, et al.** Mitochondrial dysfunction due to long-chain acyl-CoA dehydrogenase deficiency causes hepatic steatosis and hepatic insulin resistance. *Proc Natl Acad Sci USA.* 2007;104:17075–17080.
54. **Wang MY, Orci L, Ravazzola M, Unger RH.** Fat storage in adipocytes requires inactivation of leptin's paracrine activity: implications for treatment of human obesity. *Proc Natl Acad Sci USA.* 2005;102:18011–18016.
55. **Bruce CR, Hoy AJ, Turner N, et al.** Overexpression of carnitine palmitoyltransferase-1 in skeletal muscle is sufficient to enhance fatty acid oxidation and improve high-fat diet-induced insulin resistance. *Diabetes.* 2009;58:550–558.
56. **Coppari R, Bjørbæk C.** Leptin revisited: its mechanism of action and potential for treating diabetes. *Nat Rev Drug Discov.* 2012;11:692–708.
57. **Yamauchi T, Oike Y, Kamon J, et al.** Increased insulin sensitivity despite lipodystrophy in Crebbp heterozygous mice. *Nat Genet.* 2002;30:221–226.
58. **Matsumoto K, Yu S, Jia Y, et al.** Critical role for transcriptional coactivator peroxisome proliferator-activated receptor (PPAR)-binding protein/TRAP220 in liver regeneration and PPAR α ligand-induced liver tumor development. *J Biol Chem.* 2007;282:17053–17060.
59. **Louet JF, Coste A, Amazit L, et al.** Oncogenic steroid receptor coactivator-3 is a key regulator of the white adipogenic program. *Proc Natl Acad Sci USA.* 2006;103:17868–17873.
60. **Lin J, Wu PH, Tarr PT, et al.** Defects in adaptive metabolism with CNS-linked hyperactivity in PGC-1α null mice. *Cell.* 2004;119:121–135.

Endocrine Journal 2014, **61** (7), 691-696

ORIGINAL

A case of thyroid storm with a markedly elevated level of circulating soluble interleukin-2 receptor complicated by multiple organ failure and disseminated intravascular coagulation syndrome

Yoko Shimoda[1], Tetsurou Satoh[1], Hiroki Takahashi[1], Akiko Katano-Toki[1], Atsushi Ozawa[1], Takuya Tomaru[1], Norio Horiguchi[1], Kyoichi Kaira[1], Masaki Nishioka[1], Nobuyuki Shibusawa[1], Koshi Hashimoto[1], Shu Wakino[2], Masatomo Mori[1, 3] and Masanobu Yamada[1]

[1] *Department of Medicine and Molecular Science, Gunma University Graduate School of Medicine, Maebashi 371-8511, Japan*
[2] *Department of Internal Medicine, Keio University, Tokyo 160-8582, Japan*
[3] *Kitakanto Molecular Novel Research Institute for Obesity and Metabolism, Midori 379-2311, Japan*

Abstract. Thyroid storm (TS) is a life-threatening endocrine emergency. However, the pathogenesis of TS is poorly understood. A 40-year-old man was admitted to a nearby hospital with body weight loss and jaundice. Five days after a contrasted abdominal computerized tomography (CT) scan, he exhibited high fever and disturbance of consciousness. He was diagnosed with TS originating from untreated Graves' disease and was transferred to the intensive care unit (ICU) of our hospital. The patient exhibited impaired consciousness (E4V1M4 in Glasgow coma scale), high fever (39.3°C), and atrial flutter with a pulse rate 162/min, and was complicated by heart failure, acute hepatic failure, and disseminated intravascular coagulation syndrome (DIC). His circulating level of soluble interleukin-2 receptor (sIL-2R), a serum marker of an activated immune response, was highly elevated (7,416 U/mL, reference range: 135-483). Multiple organ failure (MOF) and DIC were successfully managed by multimodality treatments using inorganized iodide, glucocorticoids, antithyroid drugs, beta-blockers, and diuretics as well as an anticoagulant agent and the transfusion of platelet concentrate and fresh frozen plasma. sIL-2R levels gradually decreased during the initial treatment, but were still above the reference range even after thyroidectomy. Mild elevations in serum levels of sIL-2R have previously been correlated with thyroid hormone levels in non-storm Graves' disease. The present study demonstrated, for the first time, that circulating sIL-2R levels could be markedly elevated in TS. The marked increase in sIL-2R levels was speculated to represent an inappropriate generalized immune response that plays an unknown role in the pathogenesis of TS.

Key words: Graves' disease, Thyroid storm, Multiple organ failure, Disseminated intravascular coagulation syndrome, Soluble interleukine-2 receptor (sIL-2R)

THYROID STORM (TS) is a life-threatening endocrine emergency originating almost exclusively from uncontrolled Graves' disease, typically in the presence of some triggering conditions [1]. Due to the decompensated functions of multiple organs, TS is characterized by severe clinical manifestations including disturbance of consciousness, high fever, marked tachycardia, congestive heart failure, and gastrointestinal and hepatic disturbances [1]. Nationwide surveys recently conducted in Japan revealed that the mortality of TS was still high (10.7%) because of fatal comorbidities such as shock, Multiple organ failure (MOF), and disseminated intravascular coagulation syndrome (DIC) [2]. These surveys also reported that there was no significant difference in thyroid hormone levels between TS patients and non-storm Graves' disease patients [2]. Several pathophysiological mechanisms have been proposed for the development of TS, including 1) an acute increase in the release of thyroid hormones, 2) activation of the sympathetic nervous system, 3) presence of relative adrenal insufficiency, and 4) augmentation in the peripheral cellular response to thyroid hormones; however, the precise mechanism still remains to be elucidated [1].

Interleukin-2 (IL-2) is a type 1 cytokine produced pri-

Submitted Feb. 17, 2014; Accepted Mar. 27, 2014 as EJ14-0073
Released online in J-STAGE as advance publication Apr. 20, 2014
Correspondence to: Tetsurou Satoh, M.D., Ph.D., Department of Medicine and Molecular Science, Gunma University Graduate School of Medicine, 3-39-15 Showa-machi, Maebashi 371-8511, Japan. E-mail: tsato@gunma-u.ac.jp

marily by $CD4^+$ T cells following antigen stimulation. The proliferation and activation of various lymphocyte subsets including T cells, B cells, monocytes, macrophages, natural killer cells, and lymphokine-activated killer cells are induced when IL-2 binds its high-affinity cell surface receptor (IL-2R), which is composed of 3 subunits, IL-2Rα, IL-2Rβ, and IL-2Rγ chains [3, 4]. The α chain of IL-2R, which may be released by proteolytic cleavage from the cell surface, can be rapidly induced after T cell activation and is measurable at low levels in the sera of healthy subjects and at increased levels in various hematological and autoimmune disorders as soluble IL-2R (sIL-2R) by ELISA [5]. Serum levels of sIL-2R were previously shown to be markedly increased in hematological malignancies such as adult T cell leukemia, non-Hodgkin and Hodgkin lymphoma, and hairy cell leukemia [5, 6]. Nakase et al. proposed that hematological malignancies should be strongly suspected when a patient with a bulky mass lesion has an elevated sIL-2R level over 3,000 U/mL [6]. A mild elevation in sIL2-R has also been observed in several autoimmune disorders such as systemic lupus erythematosus and rheumatoid arthritis, and could reflect disease activities [5, 7]. Circulating sIL-2R levels have also been reported to mildly increase in autoimmune Graves' disease and were positively correlated with thyroid hormone levels, but not with anti-thyroid autoantibodies [8-10]. Mild elevations in serum sIL-2R levels have also been reported in non-immunogenic thyroid disorders including toxic nodular goiter and toxic adenoma. In contrast, circulating sIL-2R levels were shown to be significantly lower in hypothyroid patients than in normal subjects [8-10]. Taken together, the production and/or release of sIL-2R in these thyroid disorders has been considered to be positively regulated by thyroid hormones rather than reflecting the autoimmune process. Nevertheless, circulating sIL-2R levels have never been evaluated in TS.

In the present study, we described a TS case with markedly elevated sIL-2R levels complicated by MOF and DIC, and monitored changes in sIL-2R levels during the treatment.

Patient

A 40-year-old man with no apparent previous medical history or family history of thyroid disease presented to a nearby hospital in February, 2012 with a loss in appetite and body weight loss that had worsened during the last 6 months. He never drank alcohol, smoked 30 cigarettes/day, and had no history of drug abuse. A physical examination revealed severe emaciation (body mass index 12.5 kg/m^2), small diffuse goiter without ophthalmopathy, and tachycardia. Laboratory findings showed liver dysfunction with jaundice (total bilirubin 6.5 mg/dL, prothrombin time 25%, AST 87 IU/L, ALT 90 IU/L, LDH 249 IU/L, and γGTP 35 IU/L) and he was emergently admitted to the hospital. Although a contrasted abdominal CT scan was performed to evaluate the cause of his liver dysfunction, the origin remained unknown in spite of the presence of moderate amounts of ascites caused by hypoalbuminemia. Increased levels of free triiodothyronine (FT3) (15.3 pg/mL), free thyroxin (FT4) (6.3 ng/dL), and anti-TSH receptor antibody (TRAb) (>30 IU/L) and undetectable TSH (<0.002 μL) were observed, and he was diagnosed with Graves' disease. Thiamozole (MMI) (30 mg/day), potassium iodide (KI) (100 mg/day), methyldigoxin (0.1 mg/day), and furosemide (20 mg/day) were promptly initiated orally. He exhibited high fever (38.4°C), restlessness, and marked tachycardia (250/min) on the 5th hospitalized day and was diagnosed with TS. Methylprednisolone (200 mg/day) was intravenously administered and KI and MMI doses were increased to 300 mg/day and 45 mg/day, respectively. He was transferred to the ICU of our hospital on the 7th hospitalized day because his consciousness level progressively deteriorated in spite of these treatments.

On admission to the ICU, the patient exhibited impaired consciousness (E4V1M4 in Glasgow coma scale) in the absence of focal signs, high fever (39.3 °C), and atrial flutter with a pulse rate 162/min. His blood pressure was 154/82 mmHg and SpO_2 was 95% in ambient air. An ultrasonography of neck revealed a diffusely enlarged goiter (the right lobe: transverse diameter 32 mm × thickness 17.3 mm and the left lobe: transverse diameter 23.5 mm × thickness 16.4 mm) with no nodular regions. Chest radiography showed mild cardiomegaly with moderate bilateral pleural effusion, and the ejection fraction on echocardiography was decreased to 43%. Brain CT and MRI scans revealed no apparent abnormal findings except mild diffuse brain atrophy. Physical and laboratory findings further indicated that he was complicated by heart failure, hepatic failure, and disseminated intravascular coagulation syndrome (DIC) (Table 1). FT3 and FT4 levels were slightly lower than those in the former hospital. The positive hepatitis B (HB) core and HB surface antibod-

ies with undetectable HB virus (HBV) DNA indicated that the patient had a past history of unrecognized HBV hepatitis. IgM antibodies against hepatitis A virus were negative. Increased levels of γ globulins and decreased levels of serum complements caused by severe liver dysfunction with hypoalbuminemia were also noted (Table 2). Based on these clinical findings, the diagnosis of TS originating from Graves' disease was confirmed according to the diagnostic criteria of Burch and Wartofsky (115 points) [1] and the Japan Thyroid Association (JTA) [2]. The sIL-2R level, measured on day 6 because hematological malignancies were suspected due to his severe emaciation, was found to be markedly elevated (7,416 U/mL, reference range: 135-483) even after the administration of corticosteroids.

Thiamazole (30 mg/day) and hydrocortisone (200 mg/day) were intravenously administered and an inorganized iodide preparation (120 mg/day) was administered *via* a nasal tube. Systemic cooling was performed using a cooling blanket. To control heart failure with marked tachycardia, propranolol and diuretics (furosemide and carperitide) were intravenously administered. DIC was treated with nafamostat mesilate, an anticoagulant agent, and the transfusion of platelet concentrate and fresh frozen plasma. Antibiotics were not administered because no signs of bacterial infection were observed, which was confirmed by a negative blood culture and endotoxin with slightly elevated C-reactive protein levels (Tables 1 and 2). His condition was successfully managed by these multimodality treatments, and he became non-febrile, was able to hold a conversation on the second hospitalized day, and was moved to the general ward the next day. His atrial flutter spontaneously returned to a sinus rhythm on the 6th hospitalized day. Further imaging studies including a whole body CT scan and gallium 67 scintigraphy ruled out the presence of malignant hematological disorders. A complication by primary biliary cirrhosis (PBC) was suspected from the positive anti-mitochondria M2 antibody on admission (Table 1) and ursodeoxycholic acid was added from day 12. However, a histopathological examination of a liver biopsy specimen obtained on day 23 revealed acute hepatitis with cholestasis, but not PBC. Total thyroidectomy was performed on day 65 after the recovery of hepatic and cardiac functions (total bilirubin 0.7 mg/dL, albumin 4.2 g/dL, prothrombin time 86%, and BNP 110.6 pg/mL) according to the wishes of the patient. We monitored changes in sIL-2R levels and found that they gradually decreased during the initial treatment, but were still above the reference range even after thyroidectomy (Fig. 1). He was discharged from hospital after rehabilitation for severe

Table 1 Laboratory findings on admission to the ICU (1)

Cell blood count	
Hct	34.0% (40.0-52.0)
Hb	10.4 g/dL (13.2-17.3)
RBC	401 × 10^4 /μL (402-570)
WBC	4,000 /μL (4,000-9,600)
Neutro	94% (42.2-73.2)
Lymph	3% (20.1-47.3)
Plt	4.1 × 10^4 /μL (16-35)

Coagulation	
Fibrinogen	88 mg/dL (150-330)
PT	21% (70-130)
APTT	58.9 sec (27.0-39.0)
FDP	25.7 μg/mL (0.0-4.0)
D-dimer	19.3 μg/mL (0.0-1.0)
AT-III	23.5% (80-120)

Blood chemistry			
TP	7.4 g/dL (6.3-7.9)	Na	149 mEq/L (137-145)
Alb	2.3 g/dL (3.9-5.0)	K	4.0 mEq/L (3.5-4.8)
T-Bil	10.1 mg/dL (0.3-1.2)	Cl	106 mEq/L (100-107)
D-Bil	7.1 mg/dL (0.0-0.2)	Ca	8.4 mg/dL (8.9-10.5)
AST	39 IU/L (13-33)	BG	157 mg/dL (80-110)
ALT	37 IU/L (8-42)	HbA1c	5.0% (4.3-5.8)
LDH	211 IU/L (119-229)	T-Chol	64 mg/dL (128-219)
ALP	345 IU/L (115-359)	TG	58 mg/dL (30-149)
γGPT	23 IU/L (10-47)	CRP	0.94 mg/dL (<0.1)
CK	169 IU/L (62-287)	NH3	80 μg/dL (80-120)
BUN	38 mg/dL (8-20)	BNP	3,249 g/mL (0-18.4)
Cr	0.58 mg/dL (0.8-1.3)	Ferritin	81.5 ng/mL (40.7-335.8)
UA	9.5 mg/dL (3.2-7.0)	Procalcitonin	0.45 ng/mL (0-0.49)
	eGFR 102.6 ml/min/m^2	Endotoxin	negative

Hct, hematocrit; Hb, hemoglobin; RBC, red blood cell; WBC, white blood cell; Neutro, neutrophil; Lymph, lymphocyte; Plt, platelet; PT-INR, prothrombin time-international normalization ratio; APTT, activated partial thromboplastin time; FDP, fibrin/fibrinogen degradation product; AT-III, anti-thrombin III; TP, total protein; Alb, albumin; T-Bil, total bilirubin; D-Bil, direct bilirubin; AST, aspartate aminotransferase; ALT, alanine aminotransferase; LDH, lactate dehydrogenase; ALP, alkaline phosphatase; γGTP, γ-glutamyl transpeptidase; CK, creatine kinase; BUN, blood urea nitrogen; Cr, creatinine; UA, uric acid; eGFR, estimated glomerular filtration rate; BG, blood glucose; T-Chol, total cholesterol; TG, triglyceride; CRP, C-reactive protein; BNP, brain natriuretic peptide. The normal range is shown in parentheses.